October, 2004

On the equilibrium states predicted by second moment models in rotating, stably stratified homogeneous shear flow

Minsuk Ji, *Stanford University*
Paul A. Durbin, *Stanford University*

AIP | Physics of Fluids

On the equilibrium states predicted by second moment models in rotating, stably stratified homogeneous shear flow

Minsuk Ji and Paul A. Durbin

Citation: Physics of Fluids **16**, 3540 (2004); doi: 10.1063/1.1775806
View online: http://dx.doi.org/10.1063/1.1775806
View Table of Contents: http://scitation.aip.org/content/aip/journal/pof2/16/10?ver=pdfcov
Published by the AIP Publishing

On the equilibrium states predicted by second moment models in rotating, stably stratified homogeneous shear flow

Minsuk Ji and Paul A. Durbin
Department of Mechanical Engineering, Stanford University, Stanford, California 94305-3030

(Received 30 March 2004; accepted 1 June 2004; published online 10 August 2004)

The structural equilibrium behavior of the general linear second-moment closure model in a stably stratified, spanwise rotating homogeneous shear flow is considered with the aid of bifurcation analysis. A closed form equilibrium solution for the anisotropy tensor a_{ij}, dispersion tensor K_{ij}, dimensionless scalar variance $\overline{\theta^2}/k(S/S_\theta)^2$, and the ratio of mean to turbulent time scale ε/Sk is found. The variable of particular interest to bifurcation analysis, ε/Sk is shown as a function of the parameters characterizing the body forces: Ω/S (the ratio of the rotation rate to the mean shear rate) for rotation and Ri_g (the gradient Richardson number) for buoyancy; it determines the bifurcation surface in the $\varepsilon/Sk-\Omega/S-Ri_g$ space. It is shown, with the use of the closed form solution, that the Isotropization of Production model does not have a real and stable equilibrium solution when rotational and buoyant forces of certain magnitudes are simultaneously imposed on the flow. When this occurs, time integration of the turbulence model results in a diverging solution. A new set of scalar model coefficients that is consistent with experimental data, predicts turbulence decay past the critical gradient Richardson number $Ri_g^{cr}=0.25$, and ensures the existence of stable, real solutions for all combinations of rotation and buoyancy is proposed. © *2004 American Instiute of Physics*. [DOI: 10.1063/1.1775806]

I. INTRODUCTION

The combined effects of density stratification and rotation are of considerable importance in many geophysical and industrial flows. One example is turbulent flow inside internal cooling passages of a turbine blade. The flow is subject to high rate of frame rotation and significant density stratification due to severe temperature gradient. Since turbulence quantities can be greatly affected by these body forces, resulting in suppression or enhancement, the ability of a turbulence model to correctly predict these effects is crucial.

The eddy-viscosity type turbulence model, one of the most widely used turbulence models, essentially lacks the ability to naturally incorporate external forces such as frame rotation, streamline curvature, and buoyancy. Although modifications can be made to these models to simulate body force effects, they are more of an *ad hoc* approach in that they are obtained by fitting experimental data or by imitating the behavior of second-moment closure (SMC) model; see, for example, Pettersson Reif *et al.*[1] SMC models are better suited for these situations because body forces are accounted for in a systematic manner.

Bifurcation behavior of SMC models was studied by Speziale and Mac Giolla Mhuiris[2] for a homogeneous shear flow subject to frame rotation and by Speziale *et al.*[3] and Durbin and Petterson Reif[4] for elliptic flows. Bifurcation phenomena have been used as a constraint for calibrating turbulence models[5] and as a criterion for formulating algebraic SMC models;[4] Speziale *et al.*[5] calibrated their model [Speziale, Sarkar, and Gatski (SSG) model] by closely matching the bifurcation location to that of turbulence stabilization predicted by rapid distortion theory (RDT).

Durbin and Petterson Reif[4] pointed out that SMC model bifurcation is not immediately a stabilizing bifurcation; turbulence stabilization occurs past the bifurcation point at the so-called stabilization point where the ratio of turbulent production to dissipation rate is equal to 1. Beyond the stabilization point, the ratio is less than 1 and turbulence decays. Applying this result to a stably stratified, rotating homogeneous shear flow, Petterson Reif *et al.*[6] found that the Isotropization of Production (IP) model[7] prediction of turbulence stabilization by stable stratification is not consistent with laboratory observation that turbulence growth is suppressed past the critical gradient Richardson number $Ri_g^{cr}=0.25$.[8] They suggested a set of SMC model coefficients that matches the stabilization point to the critical gradient Richardson number. Abid and Habibi[9] carried out similar analyses for the Gibson and Launder (GL)[10] and SSG models. The GL model was shown to be deficient in predicting turbulence stabilization. In addition, even though it was not examined explicitly in the context of the critical gradient Richardson number, a careful study of one of the figures (Fig. 8) in their paper indicates that the SSG model possesses the same problem.

Jin *et al.*[11] studied the equilibrium states of stably stratified homogeneous flow for two-dimensional mean flow and obtained a general form of algebraic equations. They numerically evaluated the algebraic equations for shear and plain strain flow and found that the equilibrium state matches that predicted by evolution equations.

The main purposes of this paper are twofold: first is to examine, with the aid of bifurcation analysis, the equilibrium behavior of SMC models when rotation and stable stratification are combined. A closed form solution for shear flow is obtained. From this result we find that for certain ranges of

model constants no stable, real valued equilibria exist. All current versions of the general linear model fall in this range of ill posedness.

The second aim is to improve the existing SMC model by modifying scalar model coefficients. The improved model will ensure the existence of stable, real valued equilibria for combined rotation and buoyancy, have reasonable bifurcation and stabilization characteristics (guided by the critical gradient Richardson number), and be consistent with experiments and numerical simulations. The improved model, however, retains the Reynolds stress terms from an existing model. The IP model, one of the most widely used SMC models, is chosen for this purpose.

II. HOMOGENEOUS TURBULENCE IN A ROTATING FRAME

Under the assumption of homogeneity and small-scale isotropy, the transport of the kinematic Reynolds stress tensor in a rotating frame of reference is governed by

$$d_t\overline{u_iu_j} = P_{ij} + R_{ij} + B_{ij} - \frac{2}{3}\varepsilon\delta_{ij} + \phi_{ij}, \tag{1}$$

where

$$P_{ij} = -(\overline{u_iu_k}\partial_kU_j + \overline{u_ju_k}\partial_kU_i), \tag{2}$$

$$R_{ij} = -2\Omega_k^F(\epsilon_{jkl}\overline{u_iu_l} + \epsilon_{ikl}\overline{u_ju_l}), \tag{3}$$

$$B_{ij} = -\beta(g_i\overline{u_j\theta} + g_j\overline{u_i\theta}) \tag{4}$$

are the rate of production due to mean shear, frame rotation, and buoyancy, respectively. U_i and Θ are mean velocity component and temperature, u_i and θ are fluctuating velocity component and temperature, and g_i is the acceleration due to gravity in the x_i direction. The Boussinesq approximation with $\delta\rho/\rho=-\beta\delta\Theta$, where β is the coefficient of thermal expansion, has been applied. The general linear model for the pressure-strain term is written as

$$\begin{aligned}\phi_{ij} = &-C_1a_{ij}\varepsilon + k(C_2+C_3)\left(a_{ik}S_{kj} + a_{jk}S_{ki} - \tfrac{2}{3}\delta_{ij}a_{mn}S_{nm}\right)\\ &- k(C_2-C_3)(a_{ik}\Omega_{kj}^A + a_{jk}\Omega_{ki}^A)\\ &- C_4\left(B_{ij} - \tfrac{1}{3}\delta_{ij}B_{kk}\right) + \tfrac{4}{5}S_{ij}k.\end{aligned} \tag{5}$$

S_{ij} is the mean rate of strain, Ω_{ij}^A is the absolute mean vorticity tensor, and Ω_k^F is the angular velocity of the reference frame about the x_k axis,

$$S_{ij} = \tfrac{1}{2}(\partial_jU_i + \partial_iU_j), \tag{6}$$

$$\Omega_{ij}^A = \tfrac{1}{2}(\partial_jU_i - \partial_iU_j) + \epsilon_{kji}\Omega_k^F. \tag{7}$$

The transport equations of turbulent kinetic energy k and dissipation rate ε are

$$d_tk = P + B - \varepsilon, \tag{8}$$

$$d_t\varepsilon = \frac{\varepsilon}{k}[C_{\varepsilon1}(P+B) - C_{\varepsilon2}\varepsilon], \tag{9}$$

where $P=P_{kk}/2$ and $B=B_{kk}/2$. Equations (1)–(8) lead to the evolution equation for the Reynolds stress anisotropy tensor $a_{ij}=\overline{u_iu_j}/k-(2/3)\delta_{ij}$,

$$\begin{aligned}d_ta_{ij} = &-\frac{8}{15}S_{ij} + a_{ij}\frac{\varepsilon}{k}\left[1 - C_1 - \frac{(P+B)}{\varepsilon}\right]\\ &+ (C_2+C_3-1)\left(a_{ik}S_{kj} + a_{jk}S_{ki} - \frac{2}{3}\delta_{ij}a_{mn}S_{nm}\right)\\ &- (C_2-C_3-1)(a_{ik}\Omega_{kj}^A + a_{jk}\Omega_{ki}^A)\\ &+ (1-C_4)\left(\frac{B_{ij}}{k} - \frac{2}{3}\delta_{ij}\frac{B}{k}\right) - \Omega_k^F(a_{il}\epsilon_{jkl} + a_{jl}\epsilon_{ikl}).\end{aligned} \tag{10}$$

Equations (8) and (9) are combined to give the equation for inverse turbulent time scale ε/k,

$$d_t\left(\frac{\varepsilon}{k}\right) = \left(\frac{\varepsilon}{k^2}\right)[(C_{\varepsilon1}-1)(P+B) - (C_{\varepsilon2}-1)\varepsilon]. \tag{11}$$

Under homogeneous conditions, the transport of turbulent heat flux is governed by

$$d_t\overline{u_i\theta} = P_{i\theta} + R_{i\theta} + B_{i\theta} + \phi_{i\theta}, \tag{12}$$

where

$$P_{i\theta} = -\overline{u_iu_j}\partial_j\Theta - \overline{u_j\theta}\partial_jU_i, \tag{13}$$

$$R_{i\theta} = -2\epsilon_{ijk}\Omega_j^F\,\overline{u_k\theta}, \tag{14}$$

$$B_{i\theta} = -\beta g_i\overline{\theta^2} \tag{15}$$

are the rate of production due to mean temperature gradient and mean shear, frame rotation, and buoyancy, respectively. The general linear pressure-temperature gradient model is written as

$$\begin{aligned}\phi_{i\theta} = &-C_{1c}\frac{\varepsilon}{k}\overline{u_i\theta} + C_{2c}\overline{u_j\theta}\partial_jU_i + C_{3c}\overline{u_j\theta}\partial_iU_j + C_{4c}\overline{u_iu_j}\partial_j\Theta\\ &+ C_{5c}\beta g_i\overline{\theta^2}\end{aligned} \tag{16a}$$

$$\begin{aligned}= &-C_{1c}\frac{\varepsilon}{k}\overline{u_i\theta} + (C_{2c}+C_{3c})\overline{u_j\theta}S_{ij} + (C_{2c}-C_{3c})\overline{u_j\theta}\Omega_{ij}^A\\ &+ C_{4c}\overline{u_iu_j}\partial_j\Theta + C_{5c}\beta g_i\overline{\theta^2},\end{aligned} \tag{16b}$$

where the mean temperature gradient term is also included following Dakos and Gibson.[12] A simple model equation for the temperature variance is adopted which uses a constant time scale ratio C_R,

$$d_t\overline{\theta^2} = -2\overline{u_j\theta}\partial_j\Theta - C_R\frac{\varepsilon}{k}\overline{\theta^2}, \tag{17}$$

where C_R is the ratio of mechanical time scale k/ε to scalar time scale $\overline{\theta^2}/\varepsilon_\theta$ (ε_θ is the dissipation rate of $\overline{\theta^2}$). Defining a gradient-diffusion type nondimensional dispersion tensor K_{ij} suggested by Shabany and Durbin,[13]

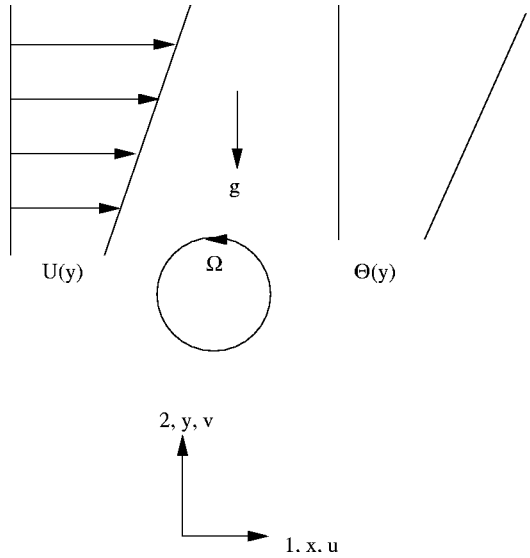

FIG. 1. Schematic of flow configuration.

$$\overline{u_i\theta} = -K_{ij}\frac{k^2}{\varepsilon}\partial_j\Theta, \tag{18}$$

Eqs. (8), (9), and (12)–(18) lead to the equation governing the evolution of the dispersion tensor K_{ij},

$$\begin{aligned}\partial_j\Theta d_t K_{ij} = {} & \partial_j\Theta K_{ij}\frac{\varepsilon}{k}\left[\frac{(P+B)}{\varepsilon}(C_{\varepsilon 1}-2)+2-C_{\varepsilon 2}\right] \\ & + K_{ij}\partial_k\Theta(S_{jk}-\Omega^A_{jk}) + (1-C_{4c})\overline{u_iu_k}\frac{\varepsilon}{k^2}\partial_k\Theta \\ & - \partial_j\Theta(1-C_{2c}+C_{3c})K_{kj}S_{ki} - \partial_j\Theta(1-C_{2c} \\ & + C_{3c})K_{kj}\Omega^A_{ki} + (1-C_{5c})\beta g_i\overline{\theta^2}\frac{\varepsilon}{k^2} \\ & - C_{1c}\frac{\varepsilon}{k}K_{ij}\partial_j\Theta - \Omega^F_l(\epsilon_{kil}\partial_j\Theta K_{kj} + \epsilon_{jkl}\partial_k\Theta K_{ij}).\end{aligned} \tag{19}$$

It should be noted that Wikström *et al.*[14] and Jin *et al.*[11] used, instead of the dispersion tensor, the nondimensional scalar flux defined as $\xi_i = \overline{u_i\theta}/\sqrt{kk_\theta}$ where $k_\theta = \overline{\theta^2}/2$ (the two can be related as $\xi_i = K_{ij}Sk/(S_\theta\varepsilon)\sqrt{2/T}\partial_j\Theta$, see below for the definition of S, S_θ, and T). As mentioned in Wikström *et al.*[14] the two approaches are similar in flows where the direction of the mean scalar gradient varies only slowly in the mean flow direction (as is the case for the present problem of vertical mean temperature gradient shown in Fig. 1) while the dispersion tensor is more appropriate in general cases such as rapidly varying mean scalar gradient. Also, the scaling used in defining the diffusivity tensor is valid for flows with passive scalar since the fluctuating temperature variance $\overline{\theta^2}$ is not required.

III. STABLY STRATIFIED SHEAR FLOW WITH SPANWISE ROTATION

The governing equations of the previous section are simplified considerably for the present problem whose mean velocity gradient tensor in the rotating frame is

$$(\partial_j U_i) = \begin{pmatrix} 0 & S & 0 \\ 0 & 0 & 0 \\ 0 & 0 & 0 \end{pmatrix},$$

the mean temperature gradient is $(\partial_i\Theta) = (0, S_\theta, 0)$, the rate of frame rotation relative to an inertial frame is $(\Omega^F_i) = (0, 0, \Omega)$, and $(g_i) = (0, -g, 0)$. Figure 1 shows the schematic of the flow configuration.

Time and turbulence quantities in the governing equations are nondimensionalized: $\overline{u_iu_j}$ and $\overline{u_i\theta}$ to a_{ij} and K_{ij}, respectively; time is nondimensionalized by the mean rate of shear S to $\tau = St$; fluctuating temperature variance $\overline{\theta^2}$ to $\overline{\theta^2}/k(S/S_\theta)^2$ (for simplicity, denoted T from now on); and the inverse turbulent time scale ε/k to ε/Sk.

The resulting set of equations is a system of seven coupled ordinary differential equations for a_{11}, a_{12}, a_{22}, K_{12}, K_{22}, ε/Sk, and T. In these equations, the effect of frame rotation and stable stratification is represented by nondimensional parameters Ω/S (the ratio of the rotation rate to the mean shear rate) and Ri_g (the gradient Richardson number), respectively. The gradient Richardson number is defined as

$$Ri_g = \frac{N^2}{S^2} = \frac{\beta g S_\theta}{S^2}, \tag{20}$$

where g is the magnitude of acceleration due to gravity, and N is the buoyancy frequency defined as $N^2 = -(g/\rho)d_2\rho = \beta g d_2\Theta$. The system of equations is

$$\begin{aligned} d_\tau a_{11} = {} & (1-C_1)\left(\frac{\varepsilon}{Sk}\right)a_{11} + a_{11}a_{12} + Ri_g\left(\frac{Sk}{\varepsilon}\right) \\ & \times\left[a_{11} + \frac{2}{3}(1-C_4)\right]K_{22} \\ & + \left[\frac{2}{3}(2C_2 - C_3 - 2) - 2(C_2 - C_3 - 2)\frac{\Omega}{S}\right]a_{12}, \end{aligned} \tag{21}$$

$$\begin{aligned} d_\tau a_{12} = {} & -\frac{4}{15} + (1-C_1)\left(\frac{\varepsilon}{Sk}\right)a_{12} + a_{12}^2 + Ri_g\left(\frac{Sk}{\varepsilon}\right)[a_{12}K_{22} \\ & - (1-C_4)K_{12}] + \left[C_3 + (C_2 - C_3 - 2)\frac{\Omega}{S}\right]a_{11} \\ & + \left[C_2 - 1 - (C_2 - C_3 - 2)\frac{\Omega}{S}\right]a_{22}, \end{aligned} \tag{22}$$

$$\begin{aligned} d_\tau a_{22} = {} & (1-C_1)\left(\frac{\varepsilon}{Sk}\right)a_{22} + a_{12}a_{22} + Ri_g\left(\frac{Sk}{\varepsilon}\right) \\ & \times\left[a_{22} - \frac{4}{3}(1-C_4)\right]K_{22} + \left[-\frac{2}{3}(C_2 - 2C_3 - 1)\right. \\ & \left. + 2(C_2 - C_3 - 2)\frac{\Omega}{S}\right]a_{12}, \end{aligned} \tag{23}$$

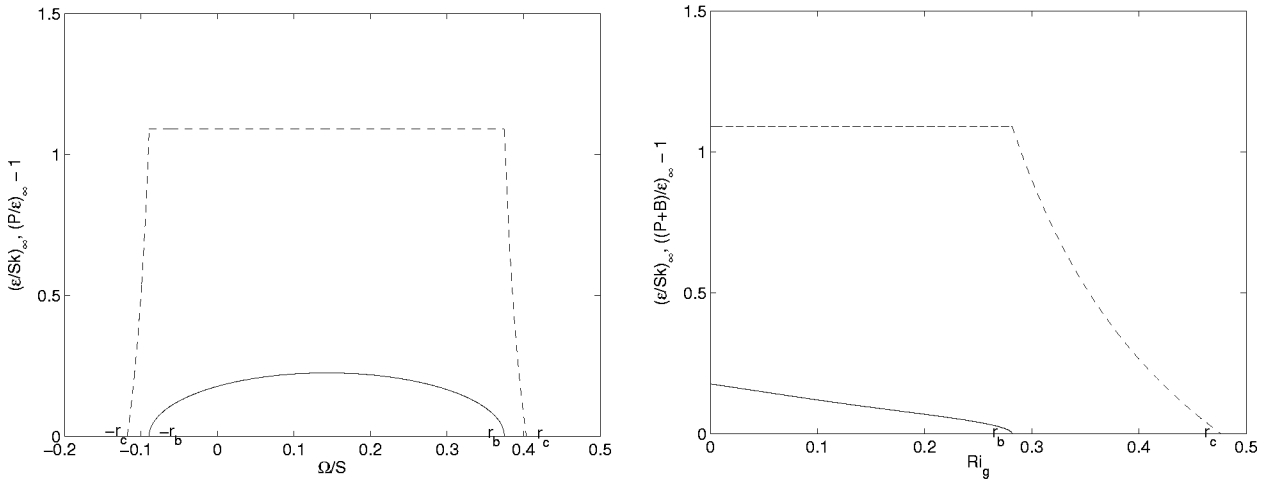

(a) Rotating homogeneous shear flow (b) Stably stratified homogeneous shear flow

FIG. 2. Bifurcation diagram for the IP model. Lines: solid, $(\varepsilon/Sk)_\infty$; dashed, $(P/\varepsilon)_\infty-1$ for (a) and $((P+B)/\varepsilon)_\infty-1$ for (b).

$$d_\tau K_{12} = (1-C_{4c})\left(\frac{\varepsilon}{Sk}\right)a_{12} - (C_{\varepsilon 1}-2)a_{12}K_{12} + (2-C_{\varepsilon 2}-C_{1c})\left(\frac{\varepsilon}{Sk}\right)K_{12} - Ri_g(C_{\varepsilon 1}-2) \times\left(\frac{Sk}{\varepsilon}\right)K_{12}K_{22} + \left[C_{2c}-1+(2-C_{2c}+C_{3c})\frac{\Omega}{S}\right]K_{22}, \tag{24}$$

$$d_\tau K_{22} = (1-C_{4c})\left(\frac{\varepsilon}{Sk}\right)\left(a_{22}+\frac{2}{3}\right) - (C_{\varepsilon 1}-2)a_{12}K_{22} + (2-C_{\varepsilon 2}-C_{1c})\left(\frac{\varepsilon}{Sk}\right)K_{22} - Ri_g\left(\frac{Sk}{\varepsilon}\right) \times(C_{\varepsilon 1}-2)K_{22}^2 - Ri_g(1-C_{5c})\left(\frac{\varepsilon}{Sk}\right)T + \left[C_{3c}-(2-C_{2c}+C_{3c})\frac{\Omega}{S}\right]K_{12}, \tag{25}$$

$$d_\tau\left(\frac{\varepsilon}{Sk}\right) = \left(\frac{\varepsilon}{Sk}\right)^2\left[(C_{\varepsilon 1}-1)\left[-\left(\frac{Sk}{\varepsilon}\right)a_{12} - Ri_g\left(\frac{Sk}{\varepsilon}\right)^2K_{22}\right] - (C_{\varepsilon 2}-1)\right], \tag{26}$$

$$d_\tau T = (1-C_R)\left(\frac{\varepsilon}{Sk}\right)T + Ta_{12} + (2+Ri_gT)\left(\frac{Sk}{\varepsilon}\right)K_{22}. \tag{27}$$

In Eq. (26),

$$\left[-\left(\frac{Sk}{\varepsilon}\right)a_{12} - Ri_g\left(\frac{Sk}{\varepsilon}\right)^2K_{22}\right] = \frac{P+B}{\varepsilon} \tag{28}$$

has been substituted into Eq. (9).

IV. STRUCTURAL EQUILIBRIUM AND BIFURCATION ANALYSES

The structural equilibrium of the Reynolds stresses is defined by $d_t a_{ij}=0$, but it requires also that $d_t(S_{ij}k/\varepsilon)=0=d_t(\Omega_{ij}^A k/\varepsilon)$.[4] The equilibrium of the Reynolds heat fluxes is defined by $d_t K_{ij}=0$ and $d_t(\partial_j\Theta)=-\partial_j U_k\partial_k\Theta=0$. For the given problem, these conditions lead to the time derivatives of ε/Sk, a_{11}, a_{12}, a_{22}, K_{12}, K_{22}, and T being 0. With their left-hand side set equal to 0, Eqs. (21)–(27) become a system of nonlinear algebraic equations which describes the state of equilibrium.

It is a particular feature of SMC models that, at equilibrium, there exist two solution branches; this is most easily seen from Eq. (26). For zero left-hand-side, either $\varepsilon/Sk=0$ (branch 2 solution) or $(P+B)/\varepsilon=(C_{\varepsilon 2}-1)/(C_{\varepsilon 1}-1)$ (branch 1 solution) is possible. The equilibrium solution bifurcates from one branch to the other as a parameter representing the external body force is varied. Along branch 1, $(P+B)/\varepsilon$ is constant at $(C_{\varepsilon 2}-1)/(C_{\varepsilon 1}-1)$ while ε/Sk is varied. The turbulent kinetic energy k grows exponentially in time: $k\propto e^{\sigma t}$ where $\sigma\propto\varepsilon/Sk$. Along branch 2, ε/Sk is 0 while $(P+B)/\varepsilon$ is varied. On this branch, k either grows or decays algebraically: $k\propto t^\lambda$ where $\lambda\propto(P+B)/\varepsilon-1$. The stabilization point, defined by $(P+B)/\varepsilon=1$, lies on the second branch. Beyond the stabilization point, $(P+B)/\varepsilon<1$ and turbulence decays. A more detailed description can be found in Durbin and Petterson Reif.[4] Figure 2 shows the bifurcation diagram of the IP model for a rotating and a stably stratified homogeneous shear flow. Bifurcation and stabilization points are labeled r_b and r_c, respectively. For a flow subject to both rotation and stratification, the bifurcation diagram is a surface over the $\Omega/S-Ri_g$ plane; the cross-section across Ω/S at a given Ri_g would look similar to Fig. 2(a) while that across Ri_g at a given Ω/S resembles Fig. 2(b).

The equilibrium solutions on the first branch are obtained from the system of nonlinear algebraic equations. One

of the variables, (ε/Sk), which is of particular interest to bifurcation analysis has four roots given by

$$\left(\frac{\varepsilon}{Sk}\right)_\infty = \pm\left[\left[(1)\left(\frac{\Omega}{S}\right)^2 + (2)\left(\frac{\Omega}{S}\right) + (3)Ri_g + (4)\right] \pm \left[(5)\left(\frac{\Omega}{S}\right)^4 + (6)\left(\frac{\Omega}{S}\right)^3 + (7)\left(\frac{\Omega}{S}\right)^2 + (8)\left(\frac{\Omega}{S}\right) + (9)Ri_g\left(\frac{\Omega}{S}\right)^2 + (10)Ri_g\left(\frac{\Omega}{S}\right) + (11)Ri_g^2 + (12)Ri_g + (13)\right]^{1/2}\right]^{1/2}, \tag{29}$$

where (1)–(13) are known functions of some of the model constants, C_1, C_2, C_3, C_4, C_{1c}, C_{2c}, C_{3c}, C_{4c}, C_{5c}, $C_{\varepsilon 1}$, $C_{\varepsilon 2}$, and C_R. The specific formulas can be found in Appendix A. The ∞ subscript is used to denote an equilibrium solution. The equilibrium solution for the other six variables is omitted for brevity.

Obtaining the second branch solution is more complicated than in the pure rotation case[2] where it was accomplished by substituting $(\varepsilon/Sk)_\infty = 0$ into the system of algebraic equations and solving for the rest of the variables. There are terms involving the inverse of ε/Sk in Eqs. (21)–(27) and hence, new variables of $O(1)$ are defined based on the asymptotic behavior of the original variables near the bifurcation point,

$$A = \left(\frac{Sk}{\varepsilon}\right)a_{12}, \quad B = \left(\frac{Sk}{\varepsilon}\right)^2 K_{22}, \quad C = \left(\frac{Sk}{\varepsilon}\right)K_{12.} \tag{30}$$

The resulting set of ordinary differential equations for the second branch is valid beyond the bifurcation point and is written as

$$d_\tau a_{11} = (A + Ri_g B - C_1 + 1)a_{11} + \left[\frac{2}{3}(2C_2 - C_3 - 2) - 2(C_2 - C_3 - 2)\frac{\Omega}{S}\right]A + \frac{2}{3}Ri_g(1 - C_4)B, \tag{31}$$

$$d_\tau A = -\frac{4}{15} + \left[C_3 + (C_2 - C_3 - 2)\frac{\Omega}{S}\right]a_{11} + \left[C_2 - 1 - (C_2 - C_3 - 2)\frac{\Omega}{S}\right]a_{22} - Ri_g(1 - C_4)C, \tag{32}$$

$$d_\tau a_{22} = (A + Ri_g B - C_1 + 1)a_{22} + \left[-\frac{2}{3}(C_2 - 2C_3 - 1) + 2(C_2 - C_3 - 2)\frac{\Omega}{S}\right]A - \frac{4}{3}Ri_g(1 - C_4)B, \tag{33}$$

$$d_\tau C = (1 - C_{4c})A + \left[C_{2c} - 1 + (2 - C_{2c} + C_{3c})\frac{\Omega}{S}\right]B + (A + Ri_g B - C_{1c} + 1)C, \tag{34}$$

$$d_\tau B = (1 - C_{4c})\left(a_{22} + \frac{2}{3}\right) + \left[C_{3c} + (C_{2c} - C_{3c} - 2)\frac{\Omega}{S}\right]C - Ri_g(1 - C_{5c})T, \tag{35}$$

$$d_\tau T = 2B + (A + Ri_g B - C_R + 1)T. \tag{36}$$

In the above equations,

$$-A - Ri_g B = \frac{P + B}{\varepsilon}. \tag{37}$$

The second branch equilibrium solutions result from Eqs. (31)–(36) with their left-hand side set equal to 0. Since the location on the second branch of the stabilization point determines when turbulence stabilizes, Eq. (37) is used in Eqs. (31)–(36) to obtain the equation for $((P+B)/\varepsilon)_\infty$ of the form,

$$0 = (1)\left(\frac{P+B}{\varepsilon}\right)_\infty^4 + (2)\left(\frac{P+B}{\varepsilon}\right)_\infty^3 + (3)\left(\frac{P+B}{\varepsilon}\right)_\infty^2 + (4)\left(\frac{P+B}{\varepsilon}\right)_\infty + (5), \tag{38}$$

where (1)–(5) are known functions of the model constants and the parameters Ω/S and Ri_g; the exact formulas can be found in Appendix B. The equilibrium solution is obtained by using the exact formula for the roots of a quartic polynomial. Due to the complexity involved in the process, however, it was evaluated numerically.

It is informative to study the equilibrium response of a model to different model constants and body forces. Consequently, solutions (29) and (38) are invaluable tools in calibrating the SMC model. The bifurcation and stabilization points are easily located on the $\Omega/S - Ri_g$ plane. Without the closed form solution, time integration to the equilibrium state would be required at many points on the plane. As will be seen in the next section, the closed form solution also helps determine whether there exists an equilibrium solution over all values of Ω/S and Ri_g.

V. MODEL CALIBRATION

Only the passive and active scalar terms in the pressure–strain and pressure–temperature gradient correlations are considered. The Reynolds stress constants are adopted from the IP model: they are $C_1 = 1.8$, $C_2 = 0.6$, $C_3 = 0$, $C_{\varepsilon 1} = 1.44$, and $C_{\varepsilon 2} = 1.92$. Speziale *et al.*[5] showed that the quasilinear SSG model performs better than the Launder, Reece and Rodi (LRR) model[15] (the IP model is similar to the LRR model) in predicting turbulence stabilization in a rotating homogeneous shear flow and that the SSG model gives better normal stress anisotropy than the LRR model; however, the linear IP model is chosen for the present analysis where the scalar terms are of main interest. With the IP model constants, the equilibrium value of the anisotropy tensor for a homogeneous shear flow is

$$(a_{ij})_\infty = \begin{pmatrix} 0.386 & -0.370 & 0 \\ -0.370 & -0.193 & 0 \\ 0 & 0 & -0.193 \end{pmatrix}. \tag{39}$$

The scalar model coefficients are calibrated based on a number of constraints: consistency with experimental and numerical simulation data for (nearly) homogeneous shear flows; agreement with the laboratory observation that turbulence stabilizes past the critical gradient Richardson number of 0.25; assurance that real, stable solutions exist when rotation and stable stratification are combined.

A. Passive scalar

The ratio of streamwise to vertical heat flux $\overline{u\theta}/\overline{v\theta}$, and the cross-correlation coefficient for the vertical heat flux $R_{v\theta}$ in homogeneous shear flows are used to calibrate passive scalar model constants. This is the same approach taken by Launder,[16] but here, the concept of structural equilibrium is used instead of his local equilibrium assumption. In addition, Launder[16] considered only C_{1c} and C_{2c} in Eq. (16a); he considered the possibility of including C_{3c} (Ref. 17) but examined it only from the "quasi-isotropic" model[18] point of view where $C_{2c}=0.8$, $C_{3c}=-0.2$ and the nonlinear "return-to-isotropy" term is required to agree with the experimental data; C_{4c} was neglected based on the ground that the mean temperature gradient term does not arise in the Poisson equation for the pressure fluctuation. However, both C_{3c} and C_{4c} are considered here since there are other constraints to be met; for example, C_{3c} plays an important role in ensuring that an equilibrium solution exists for combined rotation and stable stratification.

There are four model constants but only two kinds of calibration data, and the following approach is taken. The value for C_{1c} is selected from the range 2.5–3.2, which is a reasonable choice considering many different scalar models employ a similar value; see, for example, Table I in Wikström *et al.*[14] C_{2c} is chosen between 0.4–0.5, near that of the IP model. The remaining two constants are determined from the data. For negligible gravity effect ($Ri_g=0$), the equations for K_{ij} are decoupled from those for a_{ij} and above quantities can be written in terms of the model constants and anisotropy tensor,

$$R_{v\theta} = \frac{\overline{v\theta}}{v'\theta'} = -\sqrt{\frac{(C_R+q-1)K_{22}}{2(a_{22}+2/3)}}, \tag{40}$$

$$\frac{\overline{u\theta}}{\overline{v\theta}} = \frac{K_{12}}{K_{22}} = -\frac{(a_{22}+2/3)(C_{2c}-1)q + a_{12}^2(C_{4c}-1)(C_{1c}+q-1)}{a_{12}[(C_{4c}-1)C_{3c}q + (a_{22}+2/3)(C_{1c}+q-1)]}, \tag{41}$$

where

$$K_{22} = \frac{qC_{3c}(C_{4c}-1) + (a_{22}+2/3)(C_{1c}+q-1)}{(1-q-C_{1c})^2 - (q/a_{12})^2 C_{3c}(C_{2c}-1)}, \tag{42}$$

$v'=\sqrt{\overline{v^2}}$ and $\theta'=\sqrt{\overline{\theta^2}}$ are the rms vertical velocity and temperature fluctuations, and $q=(C_{\varepsilon 2}-1)/(C_{\varepsilon 1}-1)$. Note that a_{ij} and K_{ij} are actually equilibrium values $(a_{ij})_\infty$ and $(K_{ij})_\infty$. At the equilibrium state, $R_{v\theta}$ and $\overline{u\theta}/\overline{v\theta}$ are approximately −0.45 (Refs. 19–22) and −2.1,[19–23] respectively. Knowing from Eq. (39) the equilibrium value for the anisotropy tensor, Eqs. (40)–(42) yield $R_{v\theta}$ and $\overline{u\theta}/\overline{v\theta}$ in terms of the passive scalar model constants. The set with $C_{1c}=2.5$, $C_{2c}=0.4$, $C_{3c}=0.13$, and $C_{4c}=0$ is chosen, which gives $R_{v\theta}=-0.50$ and $\overline{u\theta}/\overline{v\theta}=-2.05$. It is pointed out that the inclusion of C_{3c}, while keeping the "return-to-isotropy" term linear, is possible if the "quasi-isotropic" model is not considered. Although there are other sets of constants that are in better agreement with the calibration data, this set is chosen because it also satisfies other constraints to be discussed in the active scalar section.

In evaluating the values for C_{1c} and C_{2c}, Launder[16] used the experimental data of Webster,[24] whose measured value for $R_{v\theta}\approx -0.45$ is correct, but $\overline{u\theta}/\overline{v\theta}\approx -1$ is not accurate. He carried out calculations assuming that local equilibrium (turbulent production $P+B$ is equal to dissipation ε) is achieved at all Ri_g and also that the time derivative of heat flux $\overline{u_i\theta}$ is 0; in the structural equilibrium analysis of the present work, $(P+B)$ is equal to ε only at the stabilization point, and the time derivative of diffusivity tensor K_{ij} is 0. When Eqs. (40)–(42) are applied, Launder's model with $C_{1c}=3.5$ and $C_{2c}=0.5$ gives $R_{v\theta}=-0.54$ and $\overline{u\theta}/\overline{v\theta}=-1.40$; the IP model employs slightly different values of $C_{1c}=2.9$ and $C_{2c}=0.4$ which yield $R_{v\theta}=-0.58$ and $\overline{u\theta}/\overline{v\theta}=-1.63$.

Turbulent Prandtl number for a nonstratified parallel shear flow, $\mathrm{Pr}_{t_o}=\nu_t/\gamma_t=(\overline{uv}S_\theta)/(\overline{v\theta}S)$ (ν_t and γ_t are turbulent viscosity and diffusivity, respectively), can be written as

$$\mathrm{Pr}_{t_o} = -\left(\frac{\varepsilon}{Sk}\right)_\infty \frac{(a_{12})_\infty}{(K_{22})_\infty} = \frac{(a_{12})_\infty^2}{q(K_{22})_\infty}, \tag{43}$$

where $(a_{12})_\infty=-q(\varepsilon/Sk)_\infty$ for a nonstratified shear flow has been used. Equation (39) gives the value of $(a_{12})_\infty$ while $(K_{22})_\infty$ is computed from Eq. (42). The new set of constants gives $Pr_{t_o}=0.71$, which falls in the acceptable range 0.5–0.9 for free shear flows.

B. Active scalar

The model constants C_4 and C_{5c} in Eqs. (5) and (16) are associated with the gravity terms. They are adjusted such that there exist real, stable equilibrium solutions and that turbulence stabilization is correctly predicted. That is the new element introduced here. It is critical to developing a model properly posed for combined effects of rotation and stratification.

1. Bifurcation characteristics and the existence of real, stable solutions

A physical solution should be both real and stable. For a bifurcating turbulence model whose equilibrium state consists of solutions from two branches, it is necessary to exam-

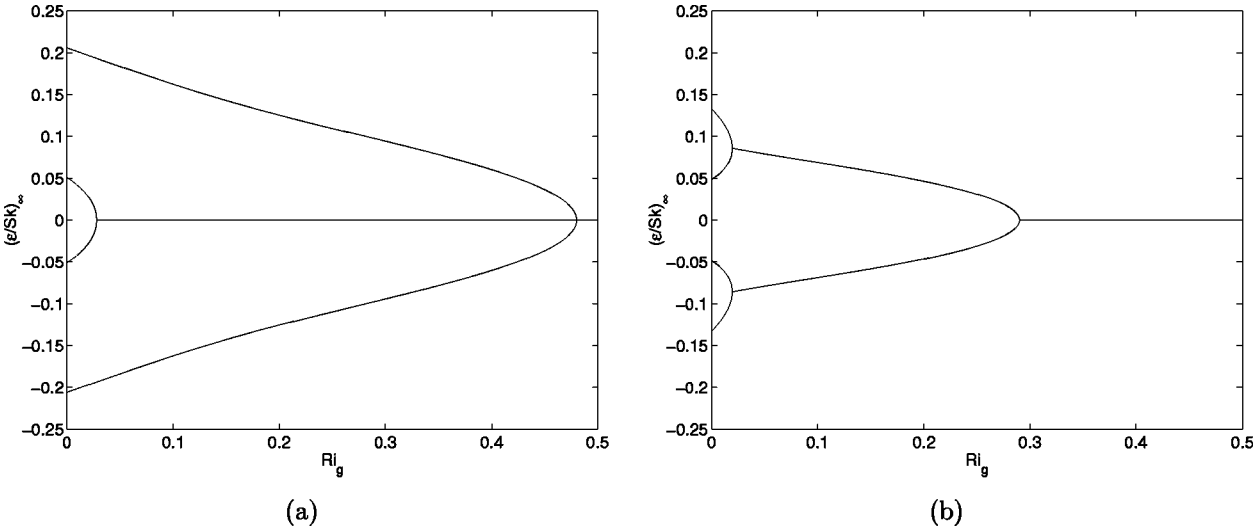

FIG. 3. Two possible bifurcation patterns when rotation and stable stratification are combined. The real part of all four roots of Eq. (29) is shown vs gradient Richardson number Ri_g at (a) $\Omega/S=0.05$, (b) $\Omega/S=0.33$.

ine the bifurcation characteristics in order to evaluate the physical soundness of the solution. Mathematically, bifurcation occurs when the first branch solution becomes imaginary. For example, a nonstratified, rotating homogeneous shear flow has a pair of first branch roots given[2] by

$$\left(\frac{\varepsilon}{Sk}\right)_\infty = \pm\frac{2(2-C_2)}{(1-q-C_1)}\left[\frac{(1-C_2)(C_1+qC_2-1)}{6q(2-C_2)^2} + \left(\frac{1-C_2}{2-C_2}\right)\frac{\Omega}{S} - \left(\frac{\Omega}{S}\right)^2\right]^{1/2}, \tag{44}$$

for the simplified form of the LRR model[15] with $C_1=1.6$ and $C_2=0.6$. Beyond a certain value of Ω/S the quantity under the square root becomes negative and the solution becomes imaginary [Fig. 2(a)].

Similarly for nonrotating stratified flow, Eq. (29) with $\Omega/S=0$ governs bifurcation. For $Ri_g<r_b$ [Fig. 2(b)], the positive root is real and stable while the negative root is real but unphysical and unstable; at the bifurcation point r_b, the two roots become an unstable imaginary pair and the second branch solution becomes a physical solution for $Ri_g>r_b$.

When buoyancy is combined with rotation, there are two pairs of roots on the first branch [Eq. (29)]. The existence of the extra pair of roots results in more than one possible bifurcation pattern, some of which are undesirable for a turbulence model. Two important bifurcation patterns are illustrated in Fig. 3 where the real part of all four roots of the IP model is shown as a function of Ri_g at a particular Ω/S. The plot for $\Omega/S=0.05$ demonstrates a desirable case: the first pair of real roots becomes an imaginary pair at $Ri_g=0.028$, as does the second pair at $Ri_g=0.481$. Since the positive root of the second pair is the stable root, bifurcation occurs at $Ri_g=0.481$. The plot for $\Omega/S=0.33$ is an undesirable case: roots of the same sign become a complex conjugate pair at $Ri_g=0.02$ and all four roots become imaginary at $Ri_g=0.291$.

This phenomenon occurs over a fairly wide range of Ω/S as can be seen from Fig. 4(a) where the contours of the real part of a positive root of Eq. (29) is shown for the IP model. The oval regions are where the first branch roots are complex. From the mathematical point of view, the oval regions occur when the argument inside the inner square root in Eq. (29) becomes negative. Figure 4(b) shows the different regimes of the two positive roots of Eq. (29).

What is the equilibrium solution and bifurcation characteristics in these regions and how do they affect the time evolution of turbulence quantities? Taking the case of $\Omega/S=0.33$ as an example, linear stability analysis indicates that the second branch solution is stable for $Ri_g>0.0068$ while the first branch solution is stable for $Ri_g<0.143$. Numerical time integration using a fourth order Runge–Kutta scheme results in a diverging solution between $Ri_g=0.02$ and 0.250. The time at which divergence occurs is as early as $\tau\approx 40$ near $Ri_g=0.02$ and as late as a few hundred τ toward $Ri_g=0.250$. Beyond 0.250, the solution is stable and evolves toward the second branch equilibrium solution. This is because the solution is attracted to the stable, but complex, branch 1 solution for $0.02\leqslant Ri_g\leqslant 0.143$. Between $Ri_g=0.143$ and 0.250, the first branch solution is only weakly unstable: two of the seven eigenvalues of the Jacobian have a positive real part whose magnitude is smaller (by an order of magnitude or by a factor of about 5) than the magnitude of the real part of the other five eigenvalues which have a negative real part; typical initial conditions (isotropic a_{ij} and K_{ij} with reasonable ε/Sk) are attracted to the complex branch 1 solution. Past $Ri_g=0.250$, the first branch solution is strongly unstable and the solution is attracted to the stable second branch solution.

This is not the correct mathematical property of a turbulence model since there is no real, stable solution when rotational and buoyant forces of certain magnitudes are combined. The bifurcation behavior is abnormal and there is a discontinuity in turbulence quantities when the switching between the two branches occurs. A new set of active scalar constants must be chosen such that there is an equilibrium

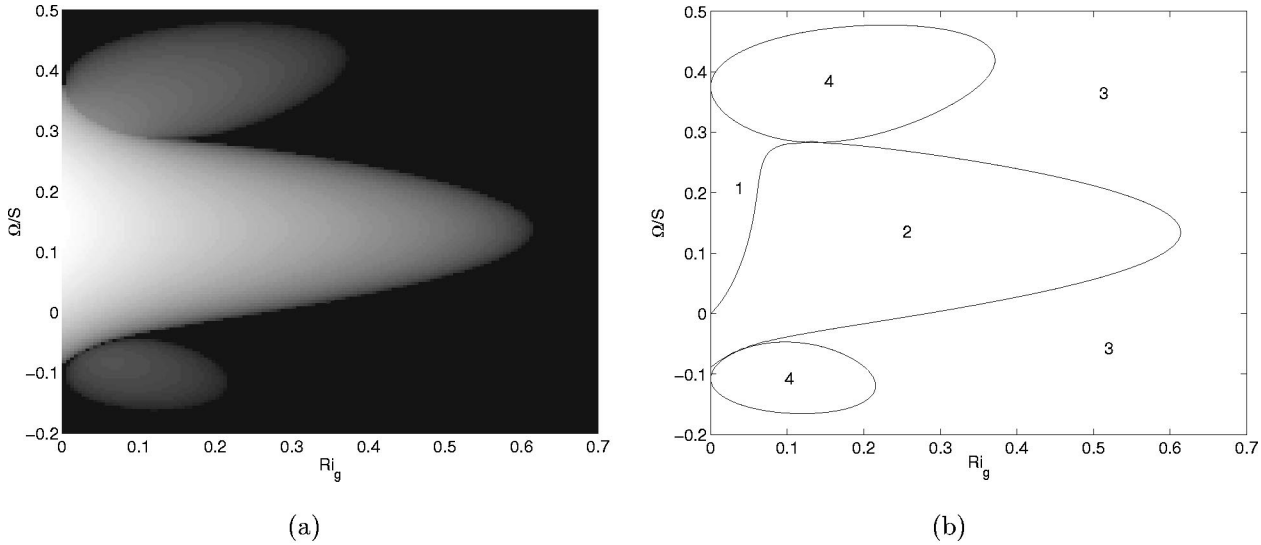

FIG. 4. Bifurcation surface for the IP model: (a) contours of the real part of a positive root of Eq. (29), (b) shows different regimes of the two positive roots of Eq. (29): 1, two real roots; 2, one real and one imaginary root; 3, two imaginary roots; 4, two complex roots.

solution over the whole region. As discussed in the preceding section, passive scalar constants are simultaneously adjusted to achieve this.

2. Critical gradient Richardson number and turbulence stabilization

The gradient Richardson number [Eq. (20)] parametrizes the stabilizing effect of stratification. Observations have shown that turbulence is suppressed beyond the critical gradient Richardson number Ri_g^{cr}. Experimental results of Rohr *et al.*[8] indicate that the critical gradient Richardson number in a stably stratified shear flow is around 0.25. Numerical simulations of Shih *et al.*[25] suggest that the critical gradient Richardson number asymptotes to 0.25 as the Reynolds number increases.

Figure 2(b) shows the bifurcation diagram of the IP model at $\Omega/S=0$. The dashed line representing $((P+B)/\varepsilon)_\infty-1$ indicates that the stabilization point is located at $Ri_g=0.48$, which is very far from $Ri_g^{cr}=0.25$. Petterson Reif *et al.*[6] imposed on SMC model the constraint that turbulence be suppressed beyond Ri_g^{cr}. They suggested a set of model constants that moved the location of stabilization to Ri_g^{cr}. The present work also aims to satisfy this constraint. It should be noted that for a rotating homogeneous shear flow Speziale and Mac Giolla Mhuiris[2] used the bifurcation point, instead of the stabilization point, to evaluate SMC model against the stability limit given by RDT. In a stably stratified homogeneous shear flow, however, it is more appropriate to use the stabilization point because the bifurcation and stabilization points are farther apart than in the rotating homogeneous shear flow. This can be seen by comparing the two plots in Fig. 2.

The proposed model constants for the active scalars are $C_4=0.32$ and $C_{5c}=0.4$. Figure 5 shows the new model's bifurcation diagram at $\Omega/S=0$ (the SMC model with the new set of constants is hereinafter referred to as the "new model" for convenience). The stabilization point is 0.246, which is close to the experimental critical gradient Richardson number. Figure 6 shows the equilibrium contours for the real part of $(\varepsilon/Sk)_\infty$. Complex solutions do not exist and the oval regions found in Fig. 4 are not present. Time integration of Eqs. (21)–(27) verifies that real, stable solutions indeed exist everywhere on the $\Omega/S-Ri_g$ plane. Figure 7 shows the locus of bifurcation and stabilization points on the $\Omega/S-Ri_g$ plane.

VI. RESULTS

Table I shows the model constants for the IP and the new model. The most notable difference is in C_4 and C_{3c}; the value of C_4 is reduced in order to meet the turbulence stabilization constraint ($Ri_g^{cr}=0.25$) and C_{3c} is mainly introduced to make sure real, stable solution exists when rotation and stable stratification are combined. Other constants are very similar to those of the IP model.

The new model can be tested in four different flow settings: (i) rotating shear flow with passive scalar, (ii) shear

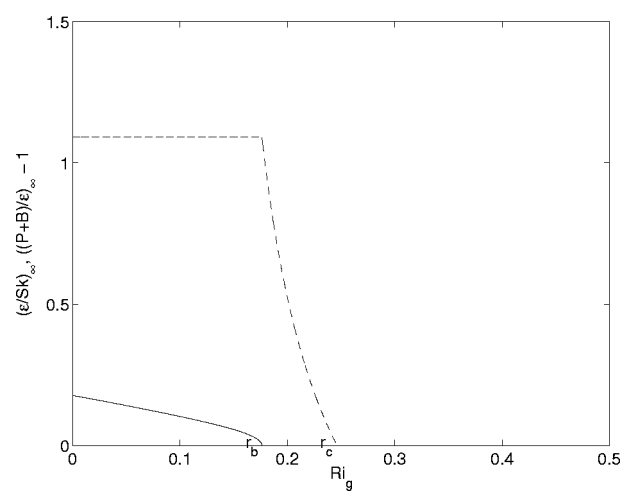

FIG. 5. Bifurcation diagram for the new model at $\Omega/S=0$. Lines: solid, $(\varepsilon/Sk)_\infty$; dashed, $((P+B)/\varepsilon)_\infty-1$.

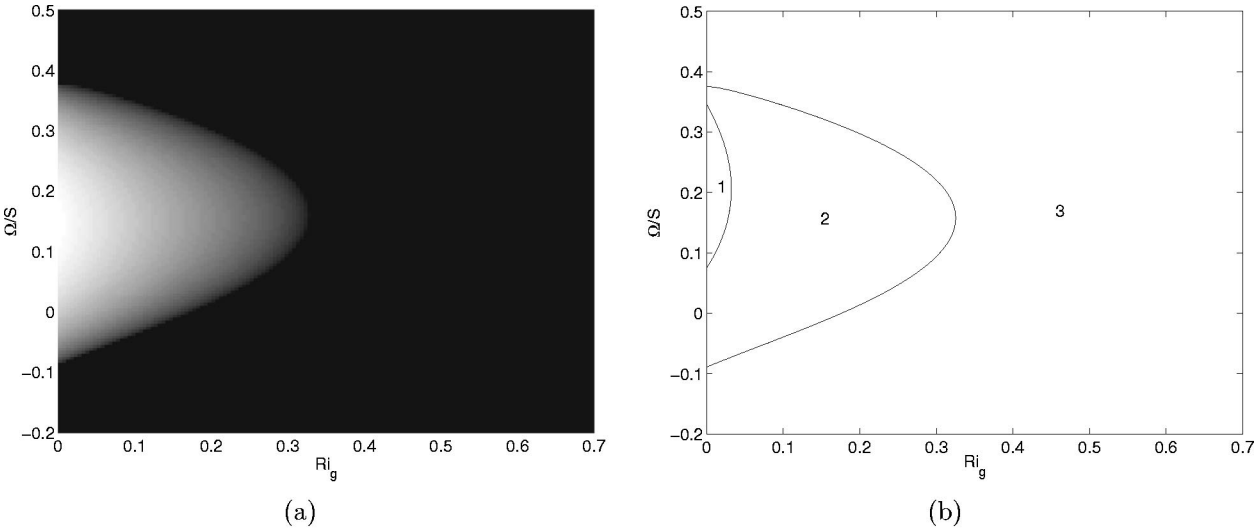

FIG. 6. Bifurcation surface for the new model: (a) contours of the real part of a positive root of Eq. (29), (b) shows different regimes of the two positive roots of Eq. (29): 1, two real roots; 2, one real and one imaginary root; 3, two imaginary roots.

flow with passive scalar, (iii) stably stratified shear flow with active scalar, and (iv) stably stratified, rotating shear flow with active scalar. However, only cases (ii) and (iii) are presently considered due to the lack of data for cases (i) and (iv); even the data on a rotating homogeneous shear flow without passive scalar is sufficiently rare that the large eddy simulations (LES) of Bardina *et al.*[26] are about the only available data. On the other hand, data on cases (ii) and (iii) are abundant. Some of them are experiments of Tavoularis and Corrsin[19] and Rohr *et al.*,[8] direct numerical simulations (DNS) of Rogers *et al.*,[23] Gerz and Schumann,[21] Holt *et al.*,[20] Shih *et al.*,[25] and Jacobitz *et al.*[27] and LES of Kaltenbach *et al.*[22]

In Fig. 8, the time evolution of normalized turbulent kinetic energy $(k/k_0)=k^*$ is shown for several gradient Richardson numbers. The rate of change of k^* in nondimensional time τ is obtained from Eqs. (8) and (28):

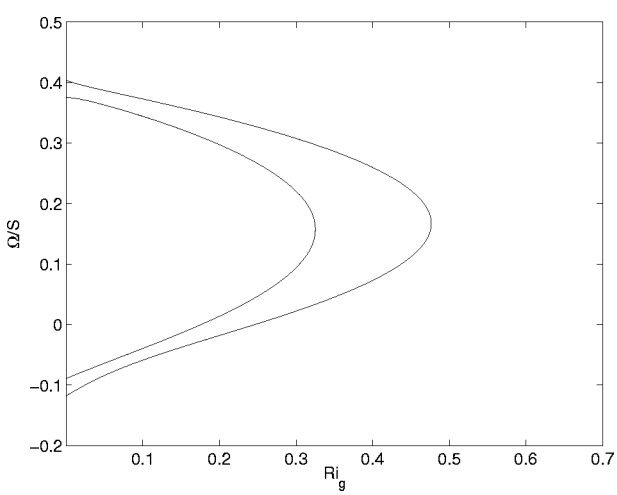

FIG. 7. Locus of bifurcation and stabilization points of the new model on the $\Omega/S-Ri_g$ plane.

$$\frac{dk^*}{d\tau}=\left(\frac{\varepsilon}{Sk}\right)\left[\frac{(P+B)}{\varepsilon}-1\right]k^*$$
$$=-\left[a_{12}+Ri_g\left(\frac{Sk}{\varepsilon}\right)K_{22}+\left(\frac{\varepsilon}{Sk}\right)\right]k^*. \tag{45}$$

As expected from the equilibrium and bifurcation analyses, both the IP and the new model predict growing turbulence for Ri_g up to the stabilization point, 0.48 and 0.25, respectively. It should be noted that the critical gradient Richardson number of 0.25 has not been obtained in any numerical simulation due to a small Reynolds number. Jacobitz *et al.*[27] shows the evolution of normalized turbulent kinetic energy in time (Fig. 5 of their paper). However, it differs from Fig. 8(b) since the critical gradient Richardson number in their simulation was 0.167. For τ less than about 10, the growth rate of turbulent kinetic energy is significantly influenced by the initial decay and therefore, it is necessary to examine the dependence of the time-evolving solution on the initial condition. The Reynolds stresses and heat fluxes were initially isotropic and 0, respectively. The amount of shear is reflected on $(\varepsilon/Sk)_0$, which was varied from 0.2 to 2.

Before considering the initial condition effect, however, the influence of Ri_g on turbulence quantities is briefly mentioned. As Ri_g increases, oscillations occur due to the increased effect of buoyancy force and the extent of these oscillations is more pronounced at earlier times when the transition from the initial isotropic state is most rapid. For more detailed description on time-evolution behavior of turbulence quantities predicted by SMC model in a stably stratified shear flow, see So *et al.*[28] The extent of oscillations also varies depending on turbulence quantities; as will be seen in this section, not much oscillation is observed for R_{uv}, $R_{v\theta}$, and $\overline{u\theta}/\overline{v\theta}$, whereas Pr_t, Ri_f, and Ri_f' show a significant amount of oscillation at early times for large Ri_g (these quatities will be defined soon). The initial condition $(\varepsilon/Sk)_0$ amplifies the effect of Ri_g. Smaller $(\varepsilon/Sk)_0$, hence larger shear

TABLE I. Model coefficients for the IP and the new model.

Constants	C_1	C_2	C_3	C_4	C_{1c}	C_{2c}	C_{3c}	C_{4c}	C_{5c}	C_R	$C_{\varepsilon 1}$	$C_{\varepsilon 2}$
IP	1.8	0.6	0.0	0.6	2.9	0.4	0.0	0.0	0.4	1.6	1.44	1.92
New	1.8	0.6	0.0	0.32	2.5	0.4	0.13	0.0	0.4	1.5	1.44	1.92

S, results in a significant increase in the amplitude of oscillation. The long time behavior, however, is hardly affected—even at large $Ri_g(\gtrsim 0.5)$; for τ large, the time-averaged value of an oscillating solution at small $(\varepsilon/Sk)_0$ is the same as the nonaveraged value of a nonoscillating solution at large $(\varepsilon/Sk)_0$.

Turbulent kinetic energy evolution is also influenced by the initial condition. Smaller $(\varepsilon/Sk)_0$ causes a decrease in both duration and amount of decay from the initial isotropic state. Again, the long time behavior of turbulent kinetic energy (especially the growth rate, or the slope of curves) is not appreciably changed. For the rest of this section, $(\varepsilon/Sk)_0 = 0.397$ is selected to agree with the initial condition used by Kaltenbach *et al.*[22] (0.397) and by Holt *et al.*[20] (0.4).

Figures 9 and 10 show model prediction of $u' = \sqrt{\overline{u^2}} = \sqrt{(a_{11}+2/3)k}$ and $v' = \sqrt{\overline{v^2}} = \sqrt{(a_{22}+2/3)k}$ with the experimental data of Rohr.[29] Taylor's hypothesis is used to represent the laboratory data (which is a function of downstream distance behind the grid) in time, $u'(\tau)$ and $v'(\tau)$. The agreement between the model prediction and experimental data is poor for $\tau < 4$; this is largely due to the difference in the duration and extent of initial decay; changing the initial condition $(\varepsilon/Sk)_0$ of the model does not improve the condition very much. Considering that the experimental data for $\tau < 4$ is under the influence of the grid,[8] the initial turbulent kinetic energy k_0 of 0.6 was chosen to match the model predictions to the corresponding experimental data for $\tau > 4$; initial condition for u' and v' was $\sqrt{0.6}$ and $\sqrt{0.3}$, respectively (note the experimental data also show initial anisotropy $u' > v'$). The agreement between the new model and the data is good for both u' and v': the slope of curves at large times matches that of experimental data. The IP model gives satisfactory results for $Ri_g = 0$ and 0.075, but less accurate results for $Ri_g = 0.21$ and 0.37. The disagreement is especially evident for u' at $Ri_g = 0.37$: the model predicts growth while decay is observed in the data. It is also seen that the IP model does a better job at large Ri_g in predicting v' than u'. Since the buoyant production B and the shear production P appear in the equation for v' and u', respectively [see, for example, Eqs. (21) and (22) in Holt *et al.*[20]], it is likely that the IP model gives more accurate B than P. This implies that one of the main reasons why the IP model over-predicts the growth rate of turbulent kinetic energy is the over-prediction of the shear production P; stratification does not directly reduce the growth of turbulent kinetic energy, but indirectly via the suppression of P.[20]

Figures 11 and 12 compare the model prediction with numerical and experimental data for the cross-correlation coefficients $R_{uv} = \overline{uv}/u'v'$ and $R_{v\theta} = \overline{v\theta}/v'\theta'$. Similarly, Fig. 13 compares the heat flux ratio $\overline{v\theta}/\overline{u\theta} = K_{22}/K_{12}$ (note that negative values of these quantities are shown in Figs. 11–13). The cross-correlation coefficients can be written as

$$R_{uv} = \frac{a_{12}}{(a_{11}+2/3)^{1/2}(a_{22}+2/3)^{1/2}}, \tag{46}$$

$$R_{v\theta} = \left(\frac{Sk}{\varepsilon}\right)\frac{K_{22}}{[T(a_{22}+2/3)]^{1/2}}. \tag{47}$$

The prediction curves are obtained by first computing from Eqs. (21)–(27) the time evolution of R_{uv}, $R_{v\theta}$, and $\overline{v\theta}/\overline{u\theta}$ for

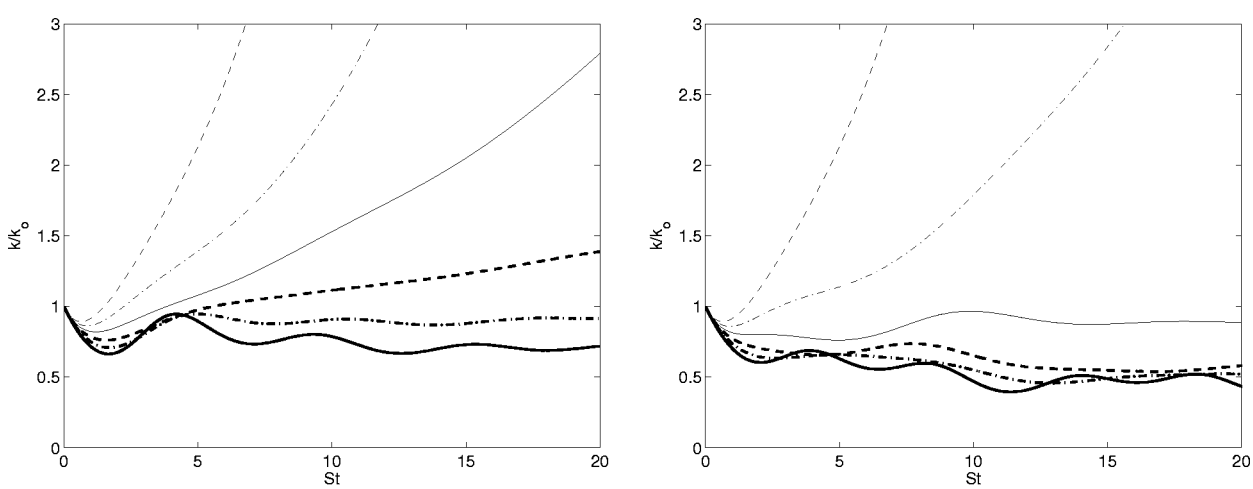

(a) IP model (b) New model

FIG. 8. Normalized turbulent kinetic energy evolution in $\tau = St$ shown at several gradient Richardson numbers. Lines: dashed, 0; dashed–dotted, 0.13; solid, 0.25; thick dashed, 0.37; thick dashed–dotted, 0.48; thick solid, 0.6.

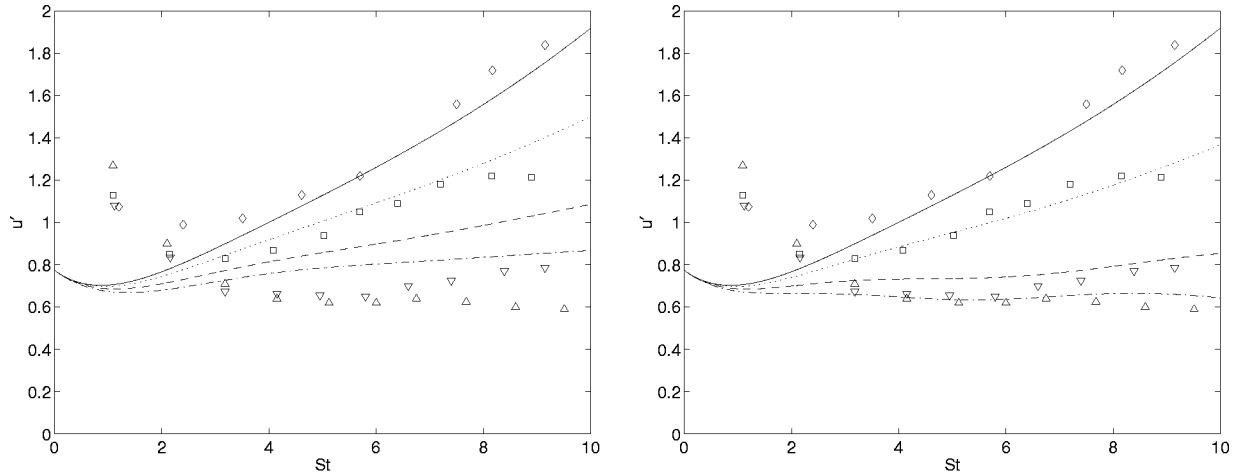

(a) IP model (b) New model

FIG. 9. u'vs St for several gradient Richardson numbers. Lines are model predictions: solid, 0; dotted, 0.075; dashed, 0.21; dashed–dotted, 0.37. Symbols are experimental results of Rohr (Ref. 29): ◇, 0; □, 0.075; ∇, 0.21; Δ, 0.37.

many gradient Richardson numbers, time averaging it around $\tau=15$, 45, 75, and 165 for each Ri_g, and then sorting the averaged data by time. Time-averaged values are used since an average value needs to be taken for oscillating solutions at large Ri_g.

From Figs. 11–13, it is seen that the effect of stable stratification is realized at lower gradient Richardson numbers in the new model; the slope of the prediction curves is steeper than that of the IP model for $0.15<Ri_g<0.25$ while the reverse is true for $0.25<Ri_g<0.4$. This is expected considering that the new model predicts turbulence stabilization at a smaller Ri_g. Turbulent kinetic energy evolution shown in Fig. 8 confirms the early influence of stable stratification in the new model. The new model's value of $R_{v\theta}$ and $\overline{v\theta}/\overline{u\theta}$ for a nonstratified flow is that obtained previously by calibrating the passive scalar model constants and, as can be seen in Figs. 12 and 13, is in better agreement with the data. All three figures indicate that the new model's prediction at $\tau=15$ fits the data relatively well (especially for $Ri_g<0.15$) while there is no single time curve from the IP model that matches the data from all three figures. Considering that most of the data were taken around $8<\tau<15$, the new model's prediction seems satisfactory.

Both models predict an immediate equilibrium for R_{uv} and $R_{v\theta}$ for Ri_g up to 0.05, while $\overline{v\theta}/\overline{u\theta}$ is a little slower to reach equilibrium even at $Ri_g=0$; the use of the equilibrium solution $(a_{ij})_\infty$ and $(K_{ij})_\infty$ in calibrating the passive scalar model constants is therefore justified. The deviation at earlier times from the equilibrium solution is most significant at $Ri_g\approx 0.2-0.3$ for the new model and at 0.3–0.4 for the IP model (prediction at $\tau=165$ can be roughly regarded as the equilibrium solution given the vertical scale of the plots).

Similar trend is found in the data shown in Figs. 11–13. For $Ri_g<0.15$ the data points are relatively close together, while a significant amount of scatter is observed for $Ri_g>0.15$ where buoyancy effect is stronger (note that nu-

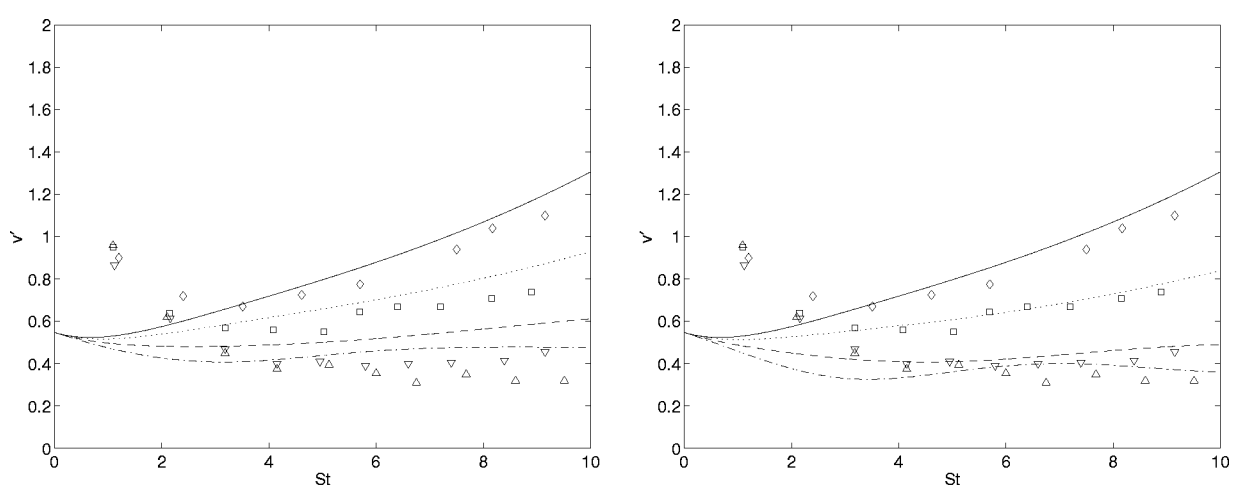

(a) IP model (b) New model

FIG. 10. v' vs St for several gradient Richardson numbers. Lines and symbols are the same as in Fig. 9.

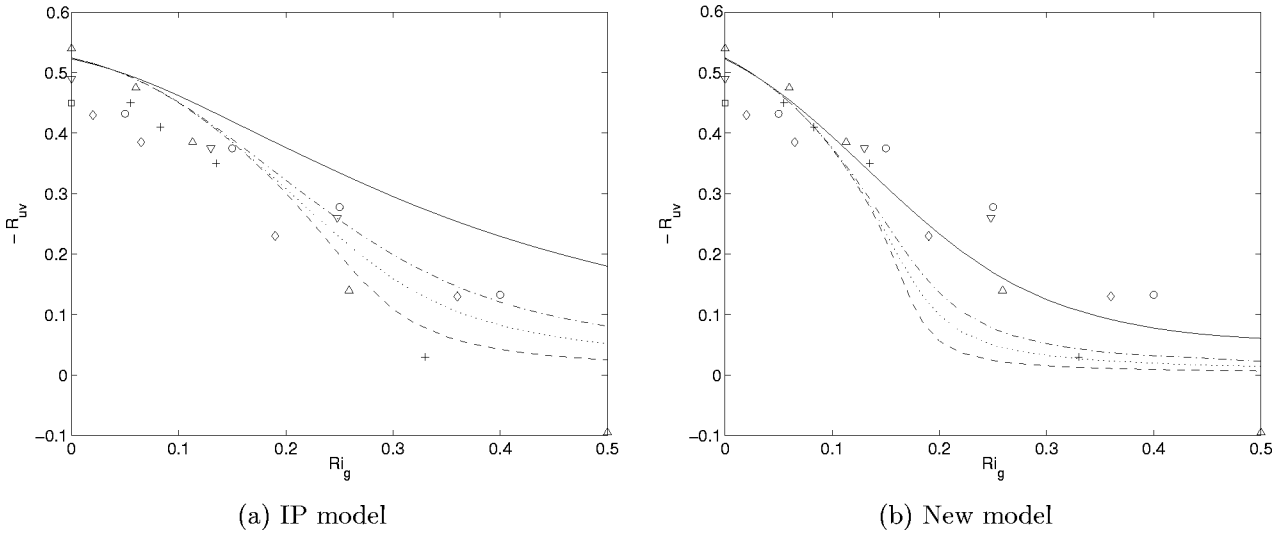

FIG. 11. Cross-correlation coefficient R_{uv} vs gradient Richardson number Ri_g. Symbols: ◇, Rohr *et al.* (Ref. 8); □, Tavoularis and Corrsin (Ref. 19); Δ, Holt *et al.* (Ref. 20); +, Gerz and Schumann (Ref. 21); ∇, Kaltenbach *et al.* (Ref. 22); ○, Shih *et al.* (Ref. 25) (private communication). Lines: solid, $\tau=15$; dashed–dotted, $\tau=45$; dotted, $\tau=75$; dashed, $\tau=165$.

merical simulations give the critical gradient Richardson number smaller than 0.25—between 0.1 and 0.2). It takes longer time to reach the equlibrium state when buoyancy effect is significant (see, for example, Tavoularis and Corrsin[19]); it is likely that the data shown in Figs. 11–13 have not reached the equilibrium state for large Ri_g. The heat flux ratio data (Fig. 13) show scatter even for $Ri_g<0.15$. This is also in accordance with the model predictions which show that for small Ri_g longer time to the equilibrium state is required for the heat flux ratio than for R_{uv} and $R_{v\theta}$.

According to experiments and numerical simulations, flow reaches the equilibrium state before $\tau\approx 15$; however, models require much longer time. Two possible answers for this discrepancy are first, as discussed in the previous paragraph, the equilibrium state might not have been reached owing to the limited duration (maximum $\tau<20$) in experiments and numerical simulations; second, it is possible that the equilibrium state predicted by SMC model is not physical: according to the SMC model, $(\varepsilon/Sk)_\infty$ is 0 after the model bifurcates and, in a strict sense, the equilibrium solution is approached only as $\tau\rightarrow\infty$. Zhao *et al.*[30] found by including a nonisotropy term in the scalar dissipation equation a nonzero $(\varepsilon/Sk)_\infty$ that reaches a constant value at some finite time. Shih *et al.*[25] found $(\varepsilon/Sk)_\infty\approx 0.18$ at $Ri_g=0.16$ for their highest Reynolds number simulations ($Ri_g=0.16$ was the stabilization point for their Reynolds number and therefore, the flow is past the bifurcation point). In geophysical applications, Freedman and Jacobson[31] found that varying $C_{\varepsilon 1}$ (as a function of Ri_g) is required in order to enforce consistency with Monin–Obukhov similarity theory of the stably stratified surface layer. Two implications of this approach are (i) varying $((P+B)/\varepsilon)_\infty$ on the first branch, and (ii) the possibility of nonzero $(\varepsilon/Sk)_\infty$ if $((P+B)/\varepsilon)_\infty$ is re-

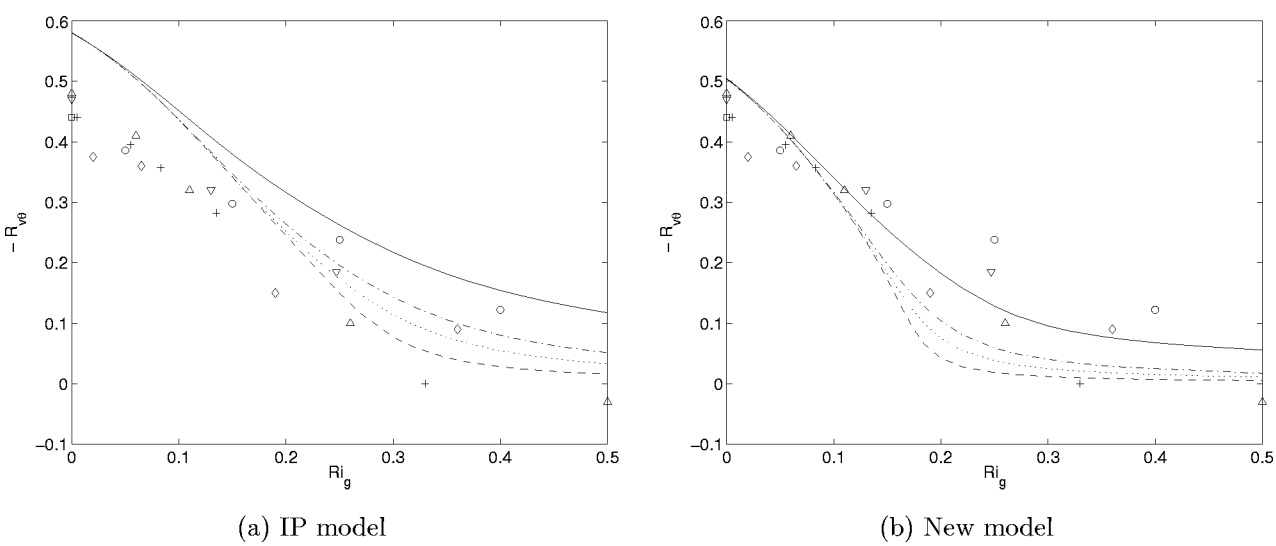

FIG. 12. Cross-correlation coefficient $R_{v\theta}$ vs gradient Richardson number Ri_g. Symbols and lines are the same as in Fig. 11.

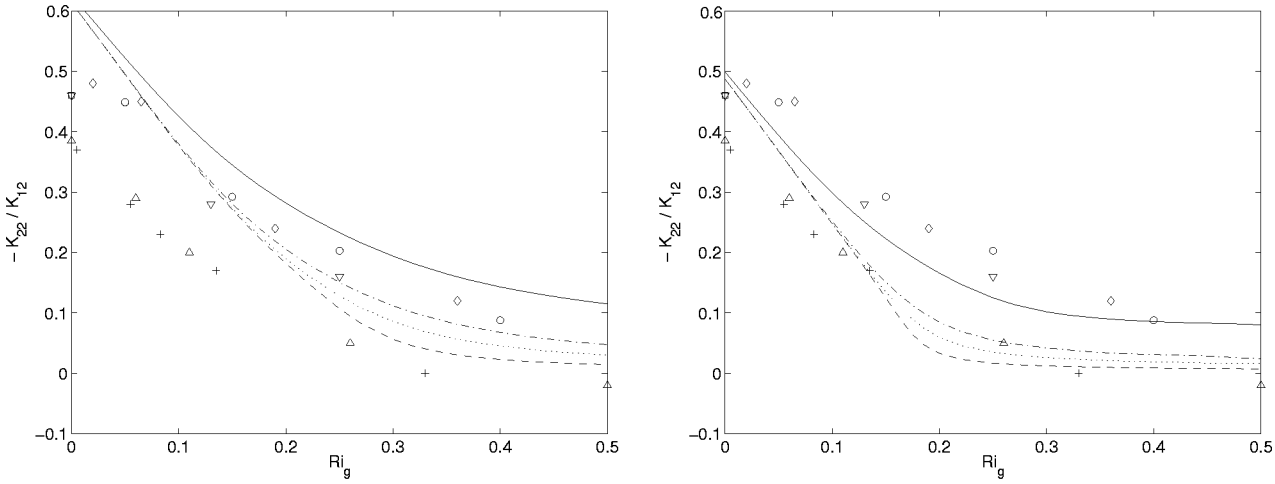

(a) IP model (b) New model

FIG. 13. Heat flux ratio $\overline{v\theta}/\overline{u\theta}$ vs gradient Richardson number Ri_g. Symbols and lines are the same as in Fig. 11.

duced to 1 before $(\varepsilon/Sk)_\infty$ becomes 0 [see Fig. 2(b) for illustration]. Variation of $((P+B)/\varepsilon)_\infty$ on the first branch is an interesting point since similar observations were made in a recent DNS of a rotating shear flow.[32] Burchard and Bolding[33] tried a separate constant $C_{\varepsilon 3}$ for the buoyancy term in the dissipation equation and found that, based on the entrainment experiment of Kato and Phillips,[34] a negative value was required. It would be of interest in the future to analyze the effect of different dissipation modeling (nonisotropy term, varying coefficients, separate coefficient for buoyancy term, etc.) on the equilibrium and bifurcation analyses and turbulence stabilization.

The flux Richardson number Ri_f is another measure that parametrizes the effect of buoyancy. It is defined as the ratio of buoyant production to shear production,

$$Ri_f = -\frac{B}{P} = \frac{\beta g \overline{v\theta}}{\overline{uv} d_y U}. \tag{48}$$

By applying the gradient-diffusion type model to both denominator and numerator, it can be shown that the ratio Ri_g/Ri_f is equivalent to the turbulent Prandtl number Pr_t, which can be written as

$$Pr_t = \frac{Ri_g}{Ri_f} = -\left(\frac{\varepsilon}{Sk}\right)\frac{a_{12}}{K_{22}}. \tag{49}$$

Figure 14 shows the model prediction of normalized turbulent Prandtl number Pr_t/Pr_{t_o} with the data from the experiments of Webster[24] and Rohr *et al.*[8] Model predictions are shown at $\tau=45$. The new model's prediction curve shows some fluctuation for $Ri_g \gtrsim 0.5$ due to strong buoyancy effect. Both models' predictions are similar for $Ri_g < 0.17$ but differ considerably for larger Ri_g; the new model has a smaller slope compared to the IP model. Even though it is difficult to tell due to the large scatter in the data which model's behavior is better, the new model's sudden slope change at $Ri_g = 0.2$ does not seem very desirable. One of the passive scalar model constants, C_{3c} has a particularly strong effect on the slope for $Ri_g > 0.2$ (through the second branch solution). However, because the constraint that real, stable solution should exist when rotation and stable stratification are combined puts a more stringent restriction on the selection of the model constants than the turbulent Prandtl number, for which the scatter in the data allows more freedom, the current set of model constants is used. Also, it should be noted that the normalized turbulent Prandtl number curve in Launder[16] was obtained by assuming local equilibrium $[(P+B)/\varepsilon=1]$ while the curves shown in Fig. 14 are obtained with structural equilibrium analysis $[(P+B)/\varepsilon=1$ at the stabilization point].

Ivey and Imberger[35] suggest the turbulent Froude number Fr_t, rather than Ri_g, for the scaling parameter for stratified flows. It is defined by $Fr_t=(\varepsilon/g'v')^{1/2}$ where $g'=g\rho'/\rho_0$, ρ' and v' are the rms density and vertical velocity fluctuations, and ρ_0 is a reference density. It can be written as

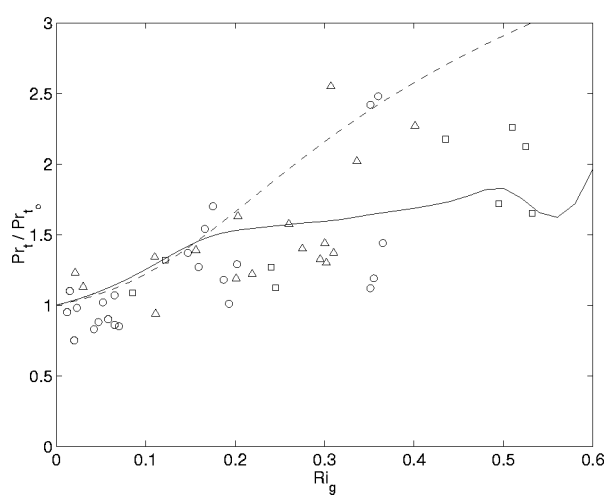

FIG. 14. Normalized turbulent Prandtl number Pr_t/Pr_{t_o} vs gradient Richardson number Ri_g. Symbols: ○, Rohr *et al.* (Ref. 8); Δ and □, Webster (Ref. 24). Lines: solid, new model at $\tau=45$; dashed, IP model at $\tau=45$.

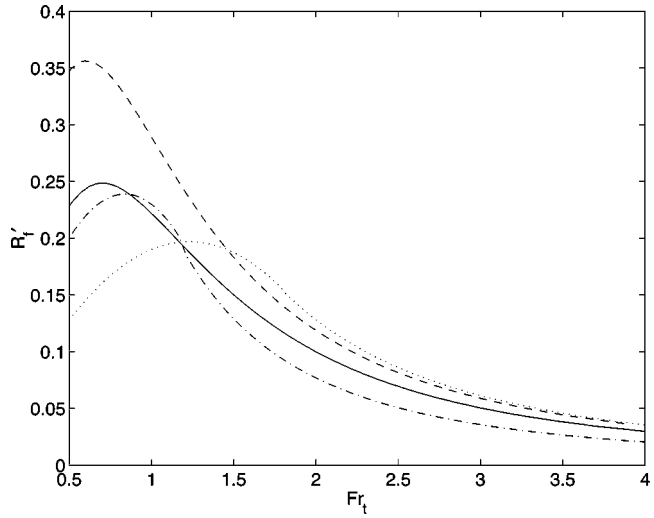

FIG. 15. Flux Richardson number Ri_f' vs turbulent Froude number Fr_t. Lines: solid, new model at $\tau=45$; dashed, IP model at $\tau=45$; dashed–dotted, Ivey and Imberger (Ref. 35) for $Pr>1$; dotted, Ivey and Imberger for $Pr<1$; infinite Reynolds number is used in the semiempirical curves.

$$Fr_t = \left[\left(\frac{\varepsilon}{Sk}\right)\frac{1}{Ri_g[T(a_{22}+2/3)]^{1/2}}\right]^{\frac{1}{2}}. \tag{50}$$

Also, the flux Richardson number is defined in a slightly different way (denoted Ri_f'):

$$Ri_f' = \frac{1}{(1-\varepsilon/B)}. \tag{51}$$

The sign of ε/B has been changed from positive in their paper to negative due to the sign difference in the definition of B. For homogeneous turbulence, Eq. (8) is used to yield

$$Ri_f' = \frac{\beta g\overline{v\theta}}{(\overline{uv}d_yU + d_tk)} = \frac{Ri_gK_{22}}{Ri_gK_{22}+(\varepsilon/Sk)^2}. \tag{52}$$

Therefore, Ri_f' is identical to Ri_f only when $d_tk=0$.

Ivey and Imberger[35] proposed a semiempirical relationship between Fr_t and Ri_f' which fits many different experimental data on stably stratified flow (both with and without shear); experimental results of Piccirillo and Van Atta[36] also supports their semiempirical curve for $Fr_t>2$. Figure 15 compares the model prediction at $\tau=45$ with the semiempirical curve, which is dependent on the turbulent Reynolds number and the molecular Prandtl number. The Reynolds stress equations do not contain the turbulent Reynolds number, which is just assumed to be large (fully turbulent). For clarity, the prediction curves are shown for $Fr_t \geqslant 0.5$ because there is a significant amount oscillation for $Fr_t<0.5$ due to strong buoyancy effects. Turbulent Froude number of 0.5 corresponds to the gradient Richardson number of about 0.39 [Eq. (50)]. Both models agree with the semiempirical curve for $Fr_t>1.3$, whereas the IP model over-predicts Ri_f' for $Fr_t<1.3$. The peak value of Ri_f' given by the new model (≈ 0.25) is comparable to that of the semiempirical curve whereas the IP model's prediction seems a little high (≈ 0.36).

VII. CONCLUDING REMARKS

The equilibrium state and bifurcation characteristics of the general linear SMC model under the influence of rotation and stable stratification have been studied. It has been demonstrated, by a closed form solution, that currently used general linear SMC models do not have a real and stable equilibrium state for certain combinations of Ω/S and Ri_g; in some regions on the $\Omega/S-Ri_g$ plane the stable equilibrium solution is complex and thus not physical. One of the passive scalar model coefficients, C_{3c} in the pressure–temperature gradient correlation has been found to have a strong influence on the existence of real and stable solution and has been modified to yield favorable results.

It has been shown that turbulence stabilization by stable stratification is not well predicted by SMC models. In order to agree with the critical gradient Richardson number constraint, one of the active scalar model coefficients, C_4 has been adjusted. Experimental and numerical simulation data have also been used to further calibrate the model coefficients.

The set of scalar model coefficients proposed in the present paper seems to give a reasonably good agreement with some of the available experiments and numerical simulations. However, the comparisons of the result section only validate the turbulence stabilization constraint. It is possible to have an SMC model that predicts turbulence stabilization correctly without making sure stable, real valued equilibria exist for combined rotation and stable stratification. This brings about a few important issues:

(i) In general, there is a large scatter in the stably stratified shear flow data (for example, in R_{uv}, $R_{v\theta}$, $\overline{v\theta}/\overline{u\theta}$, and Pr_t): the comparison presented in the result section is more appropriate as a means to see if a model predicts the trend correctly, rather than as an exclusive means to test the model's accuracy.

(ii) The bifurcation analysis is a very powerful tool in calibrating SMC models. It was found that regardless of whether a model possesses reasonably selected model coefficients or not, once a model is calibrated to match its stabilization point to the critical gradient Richardson number, its agreement with the stably stratified shear flow data is generally satisfactory. Therefore, additional constraints on SMC model are required to reduce degrees of freedom in selecting the model coefficients. For the present work, the existence of stable, real valued equilibria for combined rotation and stable stratification has been used as an additional constraint.

(iii) It would be crucial to test the new model in a rotating (both with and without stratification) homogeneous shear flow where the accuracy of its prediction of turbulent quantities can be assessed. Currently, the new model only ensures that real and stable solution exists when rotation and stable stratification are combined.

ACKNOWLEDGMENTS

The authors wish to thank Dr. Shih for providing the DNS data. This work was supported by the Department of Energy under the Accelerated Strategic Computing Initiative.

APPENDIX A: COEFFICIENTS APPEARING IN EQ. (29)

The specific formulas are as follows:

$$(1) = -\mathcal{A}/\mathcal{B}, \tag{A1}$$

$$(2) = -\mathcal{C}/\mathcal{B}, \tag{A2}$$

$$(3) = -\mathcal{D}/\mathcal{B}, \tag{A3}$$

$$(4) = -\mathcal{E}/\mathcal{B}, \tag{A4}$$

$$(5) = (\mathcal{A}^2 - 2\mathcal{B}\mathcal{F})/\mathcal{B}^2, \tag{A5}$$

$$(6) = (2\mathcal{A}\mathcal{C} - 2\mathcal{B}\mathcal{G})/\mathcal{B}^2, \tag{A6}$$

$$(7) = (2\mathcal{A}\mathcal{D} + \mathcal{C}^2 - 2\mathcal{B}\mathcal{H})/\mathcal{B}^2, \tag{A7}$$

$$(8) = (2\mathcal{C}\mathcal{D} - 2\mathcal{B}\mathcal{I})/\mathcal{B}^2, \tag{A8}$$

$$(9) = (2\mathcal{A}\mathcal{E} - 2\mathcal{B}\mathcal{J})/\mathcal{B}^2, \tag{A9}$$

$$(10) = (2\mathcal{E}\mathcal{C} - 2\mathcal{B}\mathcal{K})/\mathcal{B}^2, \tag{A10}$$

$$(11) = (\mathcal{E}^2 - 2\mathcal{B}\mathcal{L})/\mathcal{B}^2, \tag{A11}$$

$$(12) = (2\mathcal{E}\mathcal{D} - 2\mathcal{B}\mathcal{M})/\mathcal{B}^2, \tag{A12}$$

$$(13) = (\mathcal{D}^2 - 2\mathcal{B}\mathcal{N})/\mathcal{B}^2, \tag{A13}$$

where

$$\mathcal{A} = \mathrm{CD}_1 + \mathrm{AG}_1, \tag{A14}$$

$$\mathcal{B} = 2\mathrm{AC}, \tag{A15}$$

$$\mathcal{C} = \mathrm{CD}_2 - \mathrm{BE}_1 + \mathrm{AG}_2, \tag{A16}$$

$$\mathcal{D} = \mathrm{CD}_4 - \mathrm{BE}_2 + \mathrm{AG}_3, \tag{A17}$$

$$\mathcal{E} = \mathrm{CD}_3 + \mathrm{AG}_4, \tag{A18}$$

$$\mathcal{F} = \mathrm{D}_1\mathrm{G}_1, \tag{A19}$$

$$\mathcal{G} = \mathrm{D}_1\mathrm{G}_2 + \mathrm{D}_2\mathrm{G}_1 - \mathrm{E}_1\mathrm{F}_2, \tag{A20}$$

$$\mathcal{H} = \mathrm{D}_4\mathrm{G}_1 + \mathrm{D}_2\mathrm{G}_2 + \mathrm{D}_1\mathrm{G}_3 - \mathrm{E}_2\mathrm{F}_2 - \mathrm{E}_1\mathrm{F}_3, \tag{A21}$$

$$\mathcal{I} = \mathrm{D}_4\mathrm{G}_2 + \mathrm{D}_2\mathrm{G}_3 - \mathrm{E}_2\mathrm{F}_3 - \mathrm{E}_1\mathrm{F}_4, \tag{A22}$$

$$\mathcal{J} = \mathrm{D}_3\mathrm{G}_1 + \mathrm{D}_1\mathrm{G}_4 - \mathrm{E}_1\mathrm{F}_1, \tag{A23}$$

$$\mathcal{K} = \mathrm{D}_3\mathrm{G}_2 + \mathrm{D}_2\mathrm{G}_4 - \mathrm{E}_2\mathrm{F}_1 - \mathrm{E}_1\mathrm{F}_5, \tag{A24}$$

$$\mathcal{L} = \mathrm{D}_3\mathrm{G}_4, \tag{A25}$$

$$\mathcal{M} = \mathrm{D}_3\mathrm{G}_3 + \mathrm{D}_4\mathrm{G}_4 - \mathrm{E}_2\mathrm{F}_5, \tag{A26}$$

$$\mathcal{N} = \mathrm{D}_4\mathrm{G}_3 - \mathrm{E}_2\mathrm{F}_4, \tag{A27}$$

and

$$\mathrm{A} = 1 - C_1 - q, \tag{A28}$$

$$\mathrm{B} = (C_{1c} + C_{\varepsilon 2} - 2) - q(C_{\varepsilon 1} - 2), \tag{A29}$$

$$\mathrm{C} = q\mathrm{B}, \tag{A30}$$

$$\mathrm{D}_1 = 4(C_2 - C_3 - 2)^2/\mathrm{A}, \tag{A31}$$

$$\mathrm{D}_2 = -\mathrm{D}_1 - 2(C_2 - C_3 - 2)(C_4 + 1)/\mathrm{A} + (C_{2c} - C_{3c} - 2)(C_4 - 1)/\mathrm{B}, \tag{A32}$$

$$\mathrm{D}_3 = -(C_4 - 1)(C_{4c} - 1)/\mathrm{B}, \tag{A33}$$

$$\mathrm{D}_4 = 2\{(C_2 - 1)(C_2 - 2C_3 + 2C_4 - 3) - C_3(2C_2 - C_3 + C_4 - 3)\}/(3\mathrm{A}) - (C_4 - 1)(C_{2c} - 1)/\mathrm{B}, \tag{A34}$$

$$\mathrm{E}_1 = q(C_4 - 1)\{-2(C_2 - C_3 - 2)/\mathrm{A} + (C_{2c} - C_{3c} - 2)/\mathrm{B}\}, \tag{A35}$$

$$\mathrm{E}_2 = q(C_4 - 1)\{2(2C_2 - C_3 - 2)/(3\mathrm{A}) - (C_{2c} - 1)/\mathrm{B}\} - 4/15, \tag{A36}$$

$$\mathrm{F}_1 = (C_{4c} - 1)\{2(C_2 - C_3 - 2)/\mathrm{A} - (C_{2c} - C_{3c} - 2)/\mathrm{B}\}, \tag{A37}$$

$$\mathrm{F}_2 = (C_{2c} - C_{3c} - 2)^2/\mathrm{B}, \tag{A38}$$

$$\mathrm{F}_3 = -(C_{2c} - C_{3c} - 2)(C_{2c} - C_{3c} - 1)/\mathrm{B}, \tag{A39}$$

$$\mathrm{F}_4 = -C_{3c}(C_{2c} - 1)/\mathrm{B}, \tag{A40}$$

$$\mathrm{F}_5 = -2(C_{4c} - 1)(C_2 - 2C_3 + 2C_4 - 3)/(3\mathrm{A}) + 2(C_{5c} - 1)/(1 - C_R - q) - C_{3c}(C_{4c} - 1)/\mathrm{B}, \tag{A41}$$

$$\mathrm{G}_1 = q\mathrm{F}_2, \tag{A42}$$

$$\mathrm{G}_2 = q\mathrm{F}_3, \tag{A43}$$

$$\mathrm{G}_3 = q\mathrm{F}_4, \tag{A44}$$

$$\mathrm{G}_4 = -4q(C_4 - 1)(C_{4c} - 1)/(3\mathrm{A}) + 2q(C_{5c} - 1)/(1 - C_R - q) - 2(C_{4c} - 1)/3. \tag{A45}$$

APPENDIX B: COEFFICIENTS APPEARING IN EQ. (38)

Symbols appearing in this section are not related to those in Appendix A:

$$(1) = -\mathcal{AB} - \mathcal{CD}, \tag{B1}$$

$$(2) = \mathcal{ED} + \mathcal{CF} + \mathcal{GB} + \mathcal{AH}, \tag{B2}$$

$$(3) = \mathcal{ID} - \mathcal{EF} - \mathcal{CJ} - \mathcal{GH} - \mathcal{AK}, \tag{B3}$$

$$(4) = -\mathcal{IF} + \mathcal{EJ} + \mathcal{GK} - \mathcal{AL}, \tag{B4}$$

$$(5) = \mathcal{LG} + \mathcal{IJ}, \tag{B5}$$

where

$$\mathcal{A} = \mathsf{A}_1 + \mathsf{A}_3, \tag{B6}$$

$$\mathcal{B} = \mathsf{B}_5 + \mathsf{B}_6 + \mathsf{B}_7 - \mathsf{B}_4, \tag{B7}$$

$$\mathcal{C} = \mathsf{A}_2 + \mathsf{A}_4 - 4/15, \tag{B8}$$

$$\mathcal{D} = \mathsf{B}_1 + \mathsf{B}_2 + \mathsf{B}_3, \tag{B9}$$

$$\mathcal{E} = \mathsf{L}(\mathsf{A}_2 - 4/15) + \mathsf{M}(\mathsf{A}_4 - 4/15), \tag{B10}$$

$$\mathcal{F} = \mathsf{L}(\mathsf{B}_1 + \mathsf{B}_2) + \mathsf{M}(\mathsf{B}_2 + \mathsf{B}_3) + \mathsf{N}(\mathsf{B}_3 + \mathsf{B}_1), \tag{B11}$$

$$\mathcal{G} = \mathsf{A}_1\mathsf{L} + \mathsf{A}_3\mathsf{M}, \tag{B12}$$

$$\mathcal{H} = \mathsf{L}(\mathsf{B}_5 + \mathsf{B}_6 - \mathsf{B}_4) + \mathsf{M}(\mathsf{B}_5 + \mathsf{B}_7 - \mathsf{B}_4) + \mathsf{N}(\mathsf{B}_6 + \mathsf{B}_7 - \mathsf{B}_4), \tag{B13}$$

$$\mathcal{I} = 4\mathsf{LM}/15, \tag{B14}$$

$$\mathcal{J} = \mathsf{LNB}_1 + \mathsf{MNB}_3 + \mathsf{LMB}_2, \tag{B15}$$

$$\mathcal{K} = \mathsf{LM}(\mathsf{B}_5 - \mathsf{B}_4) + \mathsf{MN}(\mathsf{B}_7 - \mathsf{B}_4) + \mathsf{NL}(\mathsf{B}_6 - \mathsf{B}_4), \tag{B16}$$

$$\mathcal{L} = \mathsf{LMNB}_4, \tag{B17}$$

and

$$\mathsf{A}_1 = -(C_4 - 1)(C_{2c} - C_{3c} - 2)(\Omega/S) + (C_4 - 1)(C_{4c} - 1)Ri_g + (C_4 - 1)(C_{2c} - 1), \tag{B18}$$

$$\mathsf{A}_2 = (C_4 - 1)(C_{2c} - C_{3c} - 2)(\Omega/S) + (C_4 - 1)(C_{2c} - 1), \tag{B19}$$

$$\mathsf{A}_3 = 4(C_2 - C_3 - 2)^2(\Omega/S)^2 - 2(C_2 - C_3 - 2) \times (2C_2 - 2C_3 + C_4 - 3)(\Omega/S) + 2\{(C_2 - 1)(C_2 - 2C_3 + 2C_4 - 3) - C_3(2C_2 - C_3 + C_4 - 3)\}/3, \tag{B20}$$

$$\mathsf{A}_4 = 2(C_4 - 1)(C_2 - C_3 - 2)(\Omega/S) - 2(C_4 - 1)(2C_2 - C_3 - 2)/3, \tag{B21}$$

$$\mathsf{B}_1 = \{(C_{4c} - 1)(C_{2c} - C_{3c} - 2)(\Omega/S) + C_{3c}(C_{4c} - 1)\}Ri_g - (C_{2c} - C_{3c} - 2)^2(\Omega/S)^2 + (C_{2c} - C_{3c} - 2) \times (C_{2c} - C_{3c} - 1)(\Omega/S) + C_{3c}(C_{2c} - 1), \tag{B22}$$

$$\mathsf{B}_2 = 2(C_{5c} - 1)Ri_g, \tag{B23}$$

$$\mathsf{B}_3 = \{2(C_2 - C_3 - 2)(C_{4c} - 1)(\Omega/S) - 2(C_{4c} - 1)(C_2 - 2C_3 + 2C_4 - 3)/3\}Ri_g, \tag{B24}$$

$$\mathsf{B}_4 = -2(C_{4c} - 1)Ri_g/3, \tag{B25}$$

$$\mathsf{B}_5 = 2(C_{5c} - 1)Ri_g, \tag{B26}$$

$$\mathsf{B}_6 = -(C_{2c} - C_{3c} - 2)^2(\Omega/S)^2 + (C_{2c} - C_{3c} - 2) \times (C_{2c} - C_{3c} - 1)(\Omega/S) + C_{3c}(C_{2c} - 1), \tag{B27}$$

$$\mathsf{B}_7 = -4(C_4 - 1)(C_{4c} - 1)Ri_g/3, \tag{B28}$$

$$\mathsf{L} = 1 - C_1, \tag{B29}$$

$$\mathsf{M} = 1 - C_{1c}, \tag{B30}$$

$$\mathsf{N} = 1 - C_R. \tag{B31}$$

[1] B. A. Pettersson Reif, P. A. Durbin, and A. Ooi, "Modeling rotational effects in eddy-viscosity closures," Int. J. Heat Fluid Flow **20**, 563 (1999).
[2] C. G. Speziale and N. Mac Giolla Mhuiris, "On the prediction of equilibrium states in homogeneous turbulence," J. Fluid Mech. **209**, 591 (1989).
[3] C. G. Speziale, R. Abid, and G. A. Blaisdell, "On the consistency of Reynolds stress turbulence closures with hydrodynamic stability theory," Phys. Fluids **8**, 781 (1996).
[4] P. A. Durbin and B. A. Petterson Reif, "On algebraic second moment models," Flow, Turbul. Combust. **63**, 23 (1999).
[5] C. G. Speziale, S. Sarkar, and T. B. Gatski, "Modeling the pressure-strain correlation of turbulence: an invariant dynamical systems approach," J. Fluid Mech. **227**, 245 (1991).
[6] B. A. Petterson Reif, A. Ooi, and P. A. Durbin, "On stably stratified homogeneous shear flows subjected to rotation," Proceedings of the 2000 Summer Program, Center for Turbulence Research, Stanford University, 2000, p. 241.
[7] B. E. Launder, "Second-moment closure: present…and future?" Int. J. Heat Fluid Flow **10**, 282 (1989).
[8] J. J. Rohr, E. C. Itsweire, K. N. Helland, and C. W. Van Atta, "Growth and decay of turbulence in a stably stratified shear flow," J. Fluid Mech. **195**, 77 (1988).
[9] R. Abid and R. Habibi, "Analysis of Reynolds stress equations for stratified rotating homogeneous shear flow," Int. J. Eng. Sci. **41**, 1869 (2003).
[10] M. M. Gibson and B. E. Launder, "Ground effects on pressure fluctuations in the atmospheric boundary layer," J. Fluid Mech. **86**, 491 (1978).
[11] L. H. Jin, R. M. C. So, and T. B. Gatski, "Equilibrium states of turbulent homogeneous buoyant flows," J. Fluid Mech. **482**, 207 (2003).
[12] T. Dakos and M. M. Gibson, "On modeling the pressure terms of the scalar flux equations," in *Turbulent Shear Flows 5*, edited by F. Durst, B. E. Launder, J. L. Lumley, F. W. Schmidt, and J. H. Whitelaw (Springer, New York, 1987), p. 7.
[13] Y. Shabany and P. A. Durbin, "Explicit algebraic scalar flux approximation," AIAA J. **35**, 985 (1997).
[14] P. M. Wikström, S. Wallin, and A. V. Johansson, "Derivation and investigation of a new explicit algebraic model for the passive scalar flux," Phys. Fluids **12**, 688 (2000).
[15] B. E. Launder, G. J. Reece, and W. Rodi, "Progress in the development of a Reynolds-stress turbulence closure," J. Fluid Mech. **68**, 537 (1975).
[16] B. E. Launder, "On the effects of a gravitational field on the turbulent transport of heat and momentum," J. Fluid Mech. **67**, 569 (1975).
[17] B. E. Launder, "Heat and mass transport," in *Topics in Applied Physics*,

Vol. 12, edited by P. Bradshaw (Springer-Verlag, Berlin, 1976), p. 231.
[18] J. L. Lumley, Lecture Series No. 76, von Karman Institute, Belgium, 1975.
[19] S. Tavoularis and S. Corrsin, "Experiments in nearly homogeneous turbulent shear flows with a uniform mean temperature gradient. Part 1," J. Fluid Mech. **104**, 311 (1981).
[20] S. E. Holt, J. R. Koseff, and J. H. Ferziger, "A numerical study of the evolution and structure of homogeneous stably stratified sheard turbulence," J. Fluid Mech. **237**, 499 (1992).
[21] T. Gerz and U. Schumann, "Direct simulation of homogeneous turbulence and gravity waves in sheared and unsheared stratified flows," in *Turbulent Shear Flows 7*, edited by F. Durst, B. E. Launder, W. C. Reynolds, F. W. Schmidt, and J. H. Whitelaw (Springer, New York, 1991), p. 27.
[22] H.-J. Kaltenbach, T. Gerz, and U. Schumann, "Large-eddy simulation of homogeneous turbulence and diffusion in stably stratified shear flow," J. Fluid Mech. **280**, 1 (1994).
[23] M. M. Rogers, P. Moin, and W. C. Reynolds, "The structure and modeling of the hydrodynamic and passive scalar fields in homogeneous turbulent shear flow," Technical Report No. TF-25, Thermo-sciences Division, Department of Mechanical Engineering, Stanford University, 1986.
[24] C. A. G. Webster, "An experimental study of turbulence in a density-stratified shear-flow," J. Fluid Mech. **19**, 221 (1963).
[25] L. H. Shih, J. R. Koseff, J. H. Ferziger, and C. R. Rehmann, "Scaling and parametrization of stratified homogeneous turbulent shear flow," J. Fluid Mech. **412**, 1 (2000).
[26] J. Bardina, J. H. Ferziger, and W. C. Reynolds, "Improved turbulence models based on large eddy simulation of homogeneous, incompressible turbulent flows," Technical Report No. TF-19, Thermo-sciences Division, Department of Mechanical Engineering, Stanford University, 1983.
[27] F. G. Jacobitz, S. Sarkar, and C. W. Van Atta, "Direct numerical simulations of the turbulence evolution in a uniformly sheared and stably stratified flow," J. Fluid Mech. **342**, 231 (1997).
[28] R. M. C. So, C. Y. Zhao, and T. B. Gatski, "Predicting buoyant shear flows using anisotropic dissipation rate models," Flow, Turbul. Combust. **63**, 193 (1999).
[29] J. J. Rohr, "An experimental study of evolving turbulence in uniform mean shear flows with and without stable stratification," Ph.D. dissertation, University of California, San Diego, 1985.
[30] C. Y. Zhao, R. M. C. So, and T. B. Gatski, "Turbulence modeling effects on the prediction of equilibrium states of buoyant shear flows," Theor. Comput. Fluid Dyn. **14**, 399 (2001).
[31] F. R. Freedman and M. Z. Jacobson, "Modification of the standard ε-equation for the stable ABL through enforced consistency with Monin–Obukhov similarity theory," Boundary-Layer Meteorol. **106**, 384 (2003).
[32] "DNS and modeling of shear flow with strong rotation," 2002 Annual technical report, Center for Integrated Turbulence Simulations, Stanford University, edited by M. Fatica, W. C. Reynolds, and J. J. Alonso, p. 25.
[33] H. Burchard and K. Bolding, "Comparative analysis of four second-moment turbulence closure models for the oceanic mixed layer," J. Phys. Oceanogr. **31**, 1943 (2001).
[34] H. Kato and O. M. Phillips, "On the penetration of a turbulent layer into stratified Fluid," J. Fluid Mech. **37**, 643 (1969).
[35] G. N. Ivey and J. Imberger, "On the nature of turbulence in a stratified fluid. Part I: the energetics of mixing," J. Phys. Oceanogr. **21**, 650 (1991).
[36] P. Piccirillo and C. W. Van Atta, "The evolution of a uniformly sheared thermally stratified turbulent flow," J. Fluid Mech. **334**, 61 (1997).